Available on CMS information server

CMS NOTE 2006/104

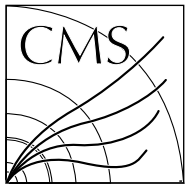

The Compact Muon Solenoid Experiment

CMS Note

Mailing address: CMS CERN, CH-1211 GENEVA 23, Switzerland

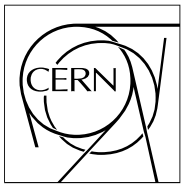

June 7, 2006

Search for Randall-Sundrum Graviton Decay into Muon Pairs

I. Belotelov, I. Golutvin, A. Lanyov, V. Palichik, E. Rogalev, M. Savina, S. Shmatov
Joint Institute for Nuclear Research, Dubna, Russia

P. Traczyk, G. Wrochna
Soltan Institute for Nuclear Studies, Warsaw, Poland

Abstract

In this work the study of Randall-Sundrum graviton decay into muon pairs has been performed. An analysis based on full detector simulation and reconstruction was carried out to derive both the CMS discovery potential for a graviton in the Randall-Sundrum scenario and the precision of a spin determination.

1 Introduction

The Standard Model (SM) has been tested in many experiments at LEP and Tevatron with a high accuracy. In particular, the yield of lepton pairs produced mainly via Drell-Yan processes, i.e. quark-antiquark annihilation by exchange of photons or Z bosons, is predicted by the SM with a per mille precision in the mass range available to the current experiments. So far, the experimental data have shown no significant deviations from SM predictions for the Drell-Yan continuum up to TeV-energy-scale.

The high-order calculations of lepton pair production cross section in the mass region of $0.1 - 0.8$ TeV are in good agreement with LEP and D0 data [1, 2]. At present, however, there are many theoretical attempts to extend the bounds of the SM in order to reach unification of strong and electroweak interactions or remove an arbitrariness in values of coupling constants in some other way and also to get rid of the known disadvantages of SM like the mass hierarchy problem, CP-violation problem etc. A quite new paradigm of gravity at TeV energies, as given in the brane world scenarios with large or compact extra spatial dimensions (ED) [3, 4], which propose a solution of the gauge hierarchy problem, has recently been discussed. In particular, these models give a set of new particles – massive Kaluza-Klein (KK) modes of the graviton which can interact with the usual matter and contribute to the SM processes causing some new interesting physics at the TeV energy scale (for more details and a phenomenology review see e.g. [5, 6]).

In our consideration we touch only one of the possible ED scenarios, the Randall-Sundrum (RS1) approach [4]. The standard setup for this approach contains two three-branes embedded into the external curved five-dimensional space-time, one (3+1)-brane with negative tension, $-\sigma$, (our world with all usual SM fields) and another one with positive tension, σ, (Planckian brane) which is needed to reproduce the SM mass hierarchy. The usual assumption is that all SM fields and fields from the Planckian sector are confined on the corresponding branes and effectively four-dimensional. The graviton is the only really multidimensional field which can freely travel through the whole space (the "bulk" space). Due to the nonzero curvature of the bulk space (which is represented by a slice of the five-dimensional anti-de-Sitter (AdS) space bounded by two branes) and the specific space-time geometry some new and very interesting physics can be realized on our brane.

In particular, in any model with compact extra spatial dimensions the graviton field will have an infinite tower of massive excitations called Kaluza-Klein (KK) modes (four-dimensional "projections" of multidimensional fields from our point of view). These modes can be visible at energies above the fundamental theory scale from energies above one or a few TeV. Then our usual massless four-dimensional graviton can be treated as the zero mode from the KK-tower. But the distinctive feature of the particular RS1 phenomenology is that excited massive graviton states (RS1 graviton) are strongly coupled to ordinary particles (not suppressed below the Planckian scale like for ordinary graviton in usual description of gravity) and can significantly contribute to the SM processes above the fundamental scale. Mass splitting between KK-modes of graviton is of the order of $\Delta m \sim k e^{-kr_c}$ [5] (where k is the curvature of the anti-de-Sitter space and r_c is compactification radius), and values of masses start from the TeV scale. So, at least the first Kaluza-Klein mode (called RS1 graviton below) can in principle be observed at the LHC as individual heavy resonance. Thus, the distinctive experimental signature for these processes is a pair of well-isolated high-p_T leptons with opposite charges coming from the same vertex.

At this point it is interesting to note that there also exist some realizations of TeV-scale gravity models where fields other than graviton can have Kaluza-Klein modes, see papers in Ref. [7]. In the papers interesting scenarios based on superstring theory were proposed in which all gauge bosons and Higgses as far as their superpartners had KK-excitations. We will not touch on such scenarios in our further discussion but we would stress that study of phenomenological consequences of the existence of KK-modes of Z^0 or photon can be done exactly in the same spirit.

Such measurements can be addressed at the CMS experiment which is able to trigger and identify the hard muons with the transverse momentum up to several TeV. The ability of the CMS experiment to detect the RS1 graviton in the di-electron and di-muon mode was investigated at first with fast reconstruction software as described in Ref. [8, 9, 10]. Full simulation and reconstruction studies in the di-electron channel were done in Ref. [11].

In this paper, the analysis of the CMS potential to observe the RS1-graviton states in the di-muon channel is presented. The Note is organized in the following way: in Chapter 2 the tools used for signal and background simulation are described, the cross sections are given. Chapter 3 is devoted to the detector response and trigger-related issues of these studies. The detailed description of the CMS performance for off-line reconstruction of di-muon pairs is also given. The main results on CMS discovery potential and analysis of angular distributions to distinguish the spin-1 state from the spin-2 states are presented in Chapters 4 and 5, respectively. Possible sources of systematic uncertainties, both theoretical- and detector-related, are discussed in Chapter 6.

2 Signal and background simulations

In assumption of a five-dimensional space in the Randall-Sundrum approach with a curvature which is of the order of Planck mass, $k \sim M_{Pl} \sim 10^{19}$ GeV, a mass spectrum of graviton spin-2 excitations (Fig. 1) is given by $m_n = kx_n e^{-kr_c\pi}$, where r_c is the compactification radius of the extra dimension and x_n are roots of the J_1 Bessel function.

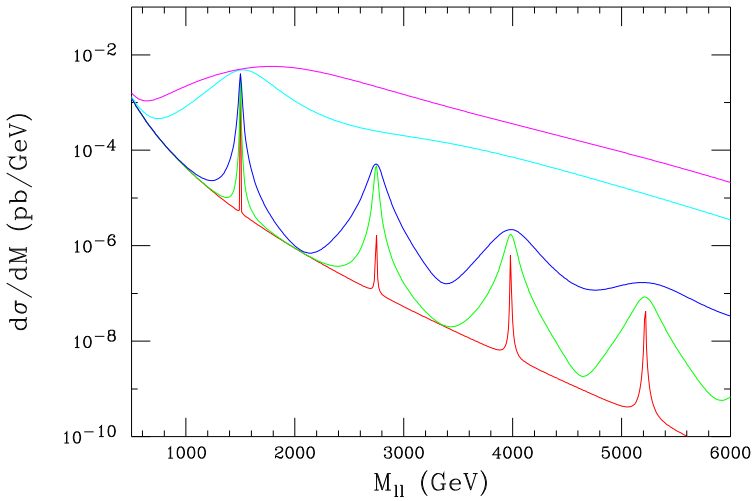

Figure 1: Invariant mass distributions for RS1 process with Drell-Yan background at the LHC. From top to bottom, the curves are for coupling values $c = 1$, 0.5, 0.1, 0.05, 0.01 (taken from [12]).

The ability to test experimentally the RS1 predictions depends on the model parameter $c = k/\bar{M}_{Pl}$ which controls the coupling of the RS1 graviton to ordinary particles and the width of the resonance:

$$\Gamma = \rho m_n x_n^2 c^2, \tag{1}$$

where the constant ρ is determined by the number of open decay channels and $\bar{M}_{Pl}$ is the effective 4-D Plank scale. In the following we use the mass of the first graviton resonance m_1 as one of the parameters of the theory, another one being the coupling constant c varied in the range $0.01 \leq c \leq 0.1$. Graviton resonances can be produced via quark-antiquark annihilation $q\bar{q} \to G_{KK}$ as well as gluon-gluon fusion $gg \to G_{KK}$. The first of these processes is identical to the Standard Model s-channel exchange by an intermediate $\gamma^\star$ or Z vector boson, while the second one has no SM analogue. The graviton production cross section is presented in Table 1 (obtained by Pythia 6.227S [13] with CTEQ6M parton distribution functions). No K factor was used for the signal. Here, two extreme possibilities for model parameter c were considered. The first one was the most optimistic scenario when c is equal to 0.1. The second set of cross sections corresponds to the most difficult for experimental observation case when the coupling constant has a value of $c = 0.01$. The width of the graviton is 1.43% for $c = 0.1$ and it is scaled as c^2 in accordance with Eq.(1). At small graviton masses ($1 - 1.5$ TeV) gluon-gluon fusion is responsible for the major part of the cross section, whereas at large graviton masses (≈ 5 TeV) $q\bar{q}$ annihilation gives the largest contribution to the cross section.

Table 1: Leading-order cross section of G_{KK} production in fb. The CTEQ6M parton distributions is used.

Contribution	$c = 0.01$				$c = 0.1$			
Mass, TeV	1.0	1.5	3.0	5.0	1.0	1.5	3.0	5.0
$gg \to G_{KK}$	6.8	0.7	0.006	0.00006	668	71	0.64	0.006
$q\bar{q} \to G_{KK}$	1.3	0.2	0.005	0.00008	134	23	0.51	0.008
Total	8.1	0.9	0.011	0.00014	812	94	1.12	0.014

The following samples have been generated using Pythia 6.227S: sixteen samples (about 10 000 events each) with $c = 0.01$, 0.02, 0.05, 0.1 for the different graviton masses $M_{G_{KK}}$ = 1.0, 1.5, 2.0, 3.0 TeV, two samples with $c = 0.01$ and 0.1 for the graviton mass $M_{G_{KK}}$ = 4.0 TeV and one sample for $c = 0.1$ and $M_{G_{KK}}$ = 5.0 TeV. All events are pre-selected for reconstruction. The branching ratio of graviton for two muons is ~ 3 %. The cross sections of graviton production for RS1 scenario are given in Table 2.

Table 2: Cross section of G_{KK} production in fb. The CTEQ6M parton distributions are used.

Mass, TeV	Value of coupling constant c				
	0.01	0.02	0.05	0.1	0.2
1.0	8.1	33	203	812	3207
1.5	0.94	3.8	23	94	359
2.0	0.18	0.7	4.3	17	67
3.0	0.012	0.046	0.29	1.1	4.5
4.0	0.0012	0.0046	0.029	0.12	0.46
5.0	0.00014	0.00055	0.0035	0.014	0.057

The background considered is Drell-Yan muon pair production, vector boson pair production ZZ, WZ, WW, $t\bar{t}$ production etc. Fourteen samples (each of ≈9000 generated events) are used for Drell-Yan background wit di-muon invariant mass cuts of 100, 150, 200, 300, 500, 1000, 1500, 2000, 2500, 3000, 3500, 4000, 4500 and 5000 GeV. The simulation and pre-selection of background events was done using Pythia 6.227 with the same cuts as for a signal above. The possible contributions from higher-order terms in the di-muon production cross section were not taking into account, a K factor of 1 was used. The total cross-sections of Drell-Yan productions for invariant masses greater than $M_{\mu^+\mu^-}$ are given in Table 3. In the SM the expected leading-order cross section of ZZ, WZ, WW, $t\bar{t}$ events is negligible in comparison with Drell-Yan one. For example, the cross-sections for di-bosons and $\mathrm{t\bar{t}}$ production with effective invariant massed greater than 1 TeV are equal to $2.59 \cdot 10^{-4}$ fb and $2.88 \cdot 10^{-4}$ fb respectively. The contribution from these processes to di-muon production falls with an invariant mass and is not taken into account in this study.

Table 3: The total leading-order cross sections of Drell-Yan production in fb. The CTEQ5L parton distributions are used, we have checked that the Drell-Yan cross sections are about the same for CTEQ6M PDFs (2–3% difference).

$M_{\mu^+\mu^-}$, TeV	1.0	1.5	2.0	2.5	3.0	4.0
Drell-Yan	6.61	$1.04 \cdot 10^{-1}$	$2.39 \cdot 10^{-1}$	$6.53 \cdot 10^{-2}$	$1.97 \cdot 10^{-2}$	$2.09 \cdot 10^{-3}$

3 Detector response and reconstruction

To simulate the particle propagation inside the detector, the GEANT4-based OSCAR package [14] was used. The digitization was performed with the CMS full-reconstruction ORCA package [15], both without a pile-up of minimum-bias collisions and with it.

The trigger simulation is realized on the basis of the ORCA package using the on-line reconstruction algorithm. For each event we have required the trigger condition for "double muon" or "single muon". This means that at least one muon candidates within the pseudorapidity region $|\eta| \leq 2.1$ is required. The Level-1 trigger performs first selection of the events, it passes only events containing two muons with a momentum greater than 3 GeV or one inclusive muon with a momentum greater 14 GeV. The efficiency of the Level-1 trigger for the samples analyzed is above 98 %.

All events accepted by the Level-1 Trigger are going to the High-Level Trigger (HLT). Muons are reconstructed by the HLT algorithms in two stages – first of all, the Level-2 algorithm using information only from the muon chambers is applied to re-evaluate the p_T of muons coming from Level-1. At the next step, at Level-3 the tracker hits are added to the muon tracks to refine the p_T measurements. The thresholds used at the muon HLT selection are 11 GeV for the HLT double muon trigger and 26 GeV for the HLT single muon trigger. Note that the trigger efficiency is significantly reduced after applying the calorimeter isolation cuts (down to 15 %). The reason for a such drop can be related with muon shower expansion with an energy due to electromagnetic radiation and interactions of a muon with the calorimeter matter. In the following, the additional cuts on calorimeter and tracker isolation are not applied at the HLT level.

The feasibility and overall performance of the muon trigger for RS1-graviton production and Drell-Yan processes are summarized in Tables 4–5. The total efficiency of triggering including L1 and HLT cuts is above 96 %, details can be found in [16]. The trigger cuts mentioned above correspond the low luminosity mode. However, values of efficiencies from Tables 4–5 are valid for larger trigger p_T cutoffs for high luminosity since the characteristic

transverse momentum of muons in the considered processes is much greater than the cutoff values.

Table 4: Trigger efficiency for Drell-Yan events at a low luminosity of 2×10^{33} cm^{-2}s^{-1}. The muons are required to be in the fiducial acceptance of the detector.

Cut for invariant mass, TeV	1.0	1.5	2.0	2.5	3.0	3.5	4.0	5.0
Level-1 + HLT	97.6	97.5	97.3	97.0	96.6	96.3	95.8	95.6

Table 5: Trigger efficiency for RS1 events at a low luminosity of 2×10^{33} cm^{-2}s^{-1}.

Graviton mass, TeV	1.0	1.5	3.0	5.0
Level-1 + HLT	97.1	96.7	95.1	94.0

For muon reconstruction, we have used a modified version of the Global Muon Reconstructor (GMR) algorithm from the ORCA package [15]. The current implementation allows to choose between different sets of hits used in the global track fitting (all the hits in the muon system, only hits in the first station, and hits in stations where an electromagnetic shower did not appear to corrupt the measurement). An option to decide between these for every reconstructed muon based on goodness-of-fit variables is also available. Studies have shown that optimal performance for high energy muons is achieved by slightly altered code selecting between only two sets of muon hits (first muon station or stations without showers). After muon reconstruction, photons in a 0.1 $\eta - \phi$ cone around every muon track are searched for, and if found, the four-momentum of the closest one is added to that of the muon. These photons come mainly from final-state radiation from the graviton decay vertex, and taking them into account improves the determination of the graviton mass (see Fig. 8). At least two off-line reconstructed muons with opposite charge signs were required, and the off-line reconstruction algorithm was applied only to events which passed the trigger selection.

The two examples of the off-line reconstructed invariant-mass spectrum for signal plus background (graviton + Drell-Yan) and background only (Drell-Yan events) are given in Fig. 2 b) and d) for $M_{inv} = 1.5$ TeV with $c = 0.01$ and $c = 0.1$, respectively, the generated spectrum can be seen for comparison in left-hand plots a) and c). The analogous plots for $M_{inv} = 3.0$ TeV are given in Fig. 3. Figs. 23–28 present plots of reconstructed di-muon invariant mass for various integrated luminosities and parameters of the model.

An example of fitted mass resolution plot for the RS1-gravitons with $m = 1.5$ TeV and $m = 3.0$ TeV for $c = 0.1$ is given in Fig. 4, the dependence on mass is shown in Fig. 5 a). For graviton mass interval $1 < m < 5$ TeV the mass resolution is between 3% and 5.6%. The curve for $c = 0.01$ practically coincides with the former one. The off-line reconstruction efficiency for di-muon events after HLT is shown in Fig. 5b) as a function of the resonance mass. Thus, the overall efficiency of fully-reconstruction procedure with taking into account an acceptance, trigger and off-line reconstruction inefficiency is above 88 % for the the graviton mass up to 5 TeV.

An example of the main kinematic distributions of muons coming from RS1-graviton decay is shown in Fig. 6. One observes that both the pseudorapidity and azimuthal angle reconstructed distributions are in a good agreement with generated ones. For transverse momentum there is some smearing of muon near the narrow peak in its spectrum.

4 Analysis

In this section, the CMS reach for detection of RS1 gravitons and results for spin state discrimination are presented.

4.1 CMS Discovery Limit

Various significance estimators have been proposed in the literature [17, 18], ranging from the estimators counting the number of the signal and background events in a certain mass range around the observed peak to estimators using ratio of likelihoods of fits with a signal+background hypothesis and with a pure background hypothesis. Each method has its advantages and drawbacks [17, 18], which is not discussed in this note, the official recommendation for the usage in CMS PRS group was to use S_{cP} (counting method) and/or S_L estimator (likelihood fitting method).

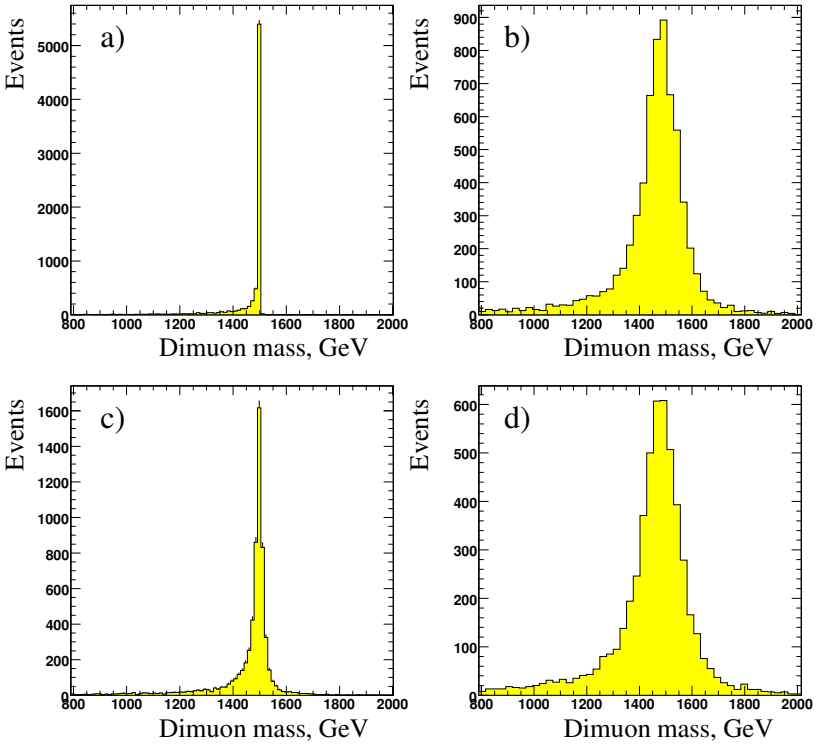

Figure 2: The reconstructed and generated invariant mass spectrum of the RS1 events over Standard Model continuum for $M_{inv} = 1.5$ TeV: a) generated events with $c = 0.01$, b) reconstructed events with $c = 0.01$, c) generated events with $c = 0.1$, d) reconstructed events with $c = 0.1$.

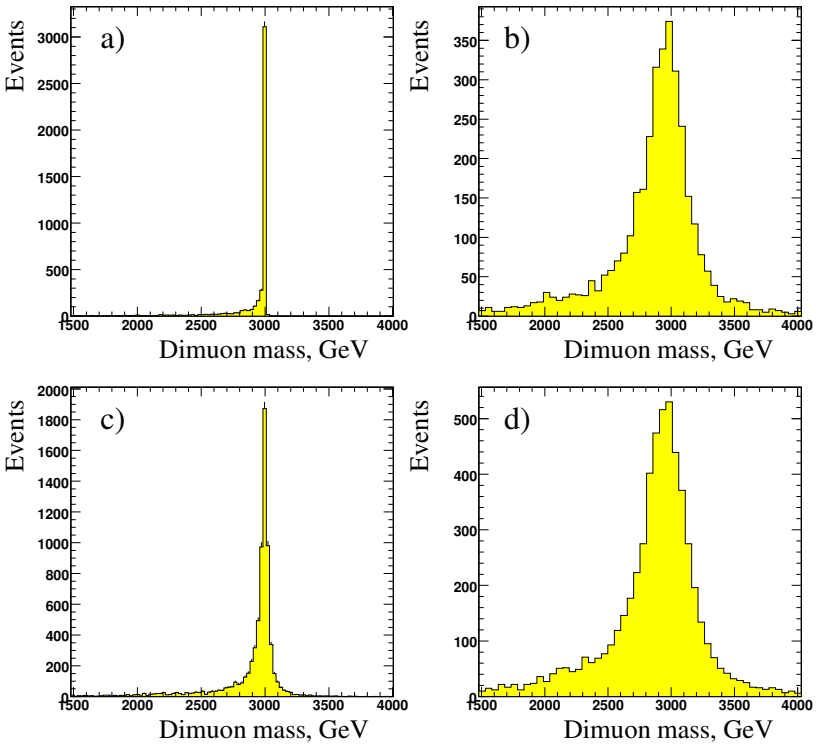

Figure 3: The reconstructed and generated invariant mass spectrum of the RS1 events over Standard Model continuum for $M_{inv} = 3.0$ TeV: a) generated events with $c = 0.01$, b) reconstructed events with $c = 0.01$, c) generated events with $c = 0.1$, d) reconstructed events with $c = 0.1$.

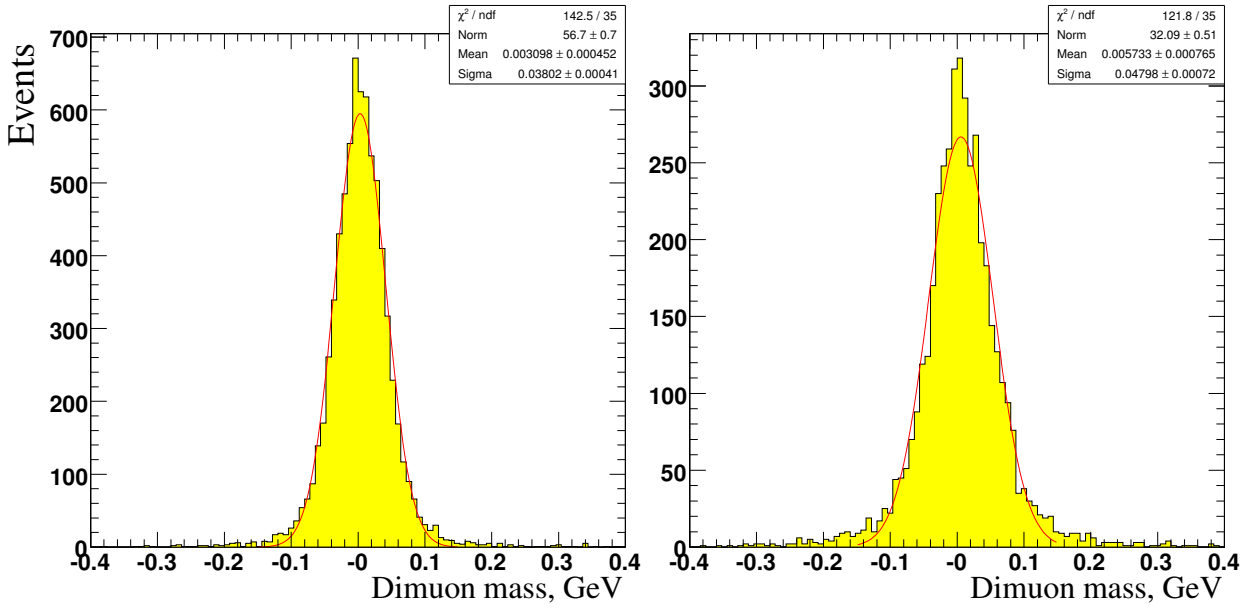

Figure 4: Mass resolution for RS1 model for $c = 0.01$ and $m = 1500$ and 3000 GeV (left and right plot, respectively).

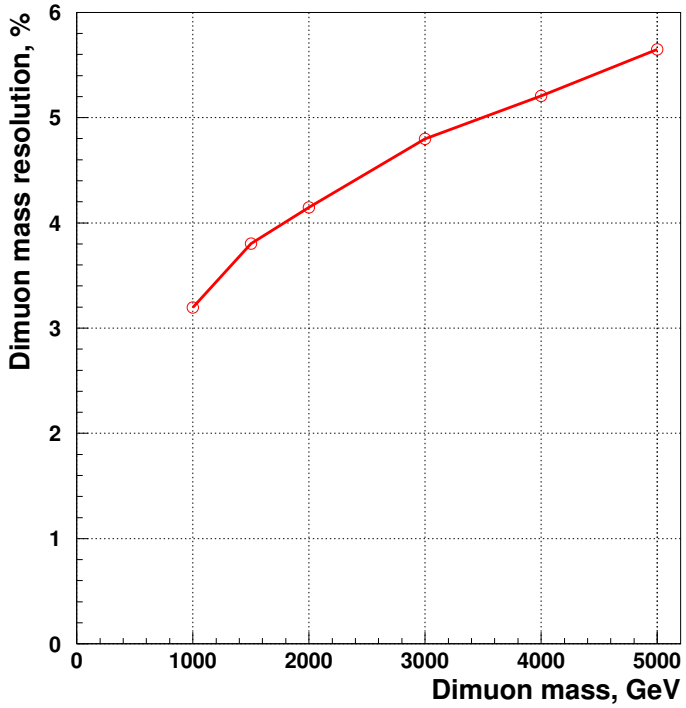

Figure 5: Dependence of mass resolution (in percent) on the generated mass in the RS1 model for $c = 0.1$. The curve for $c = 0.01$ practically coincides with this one.

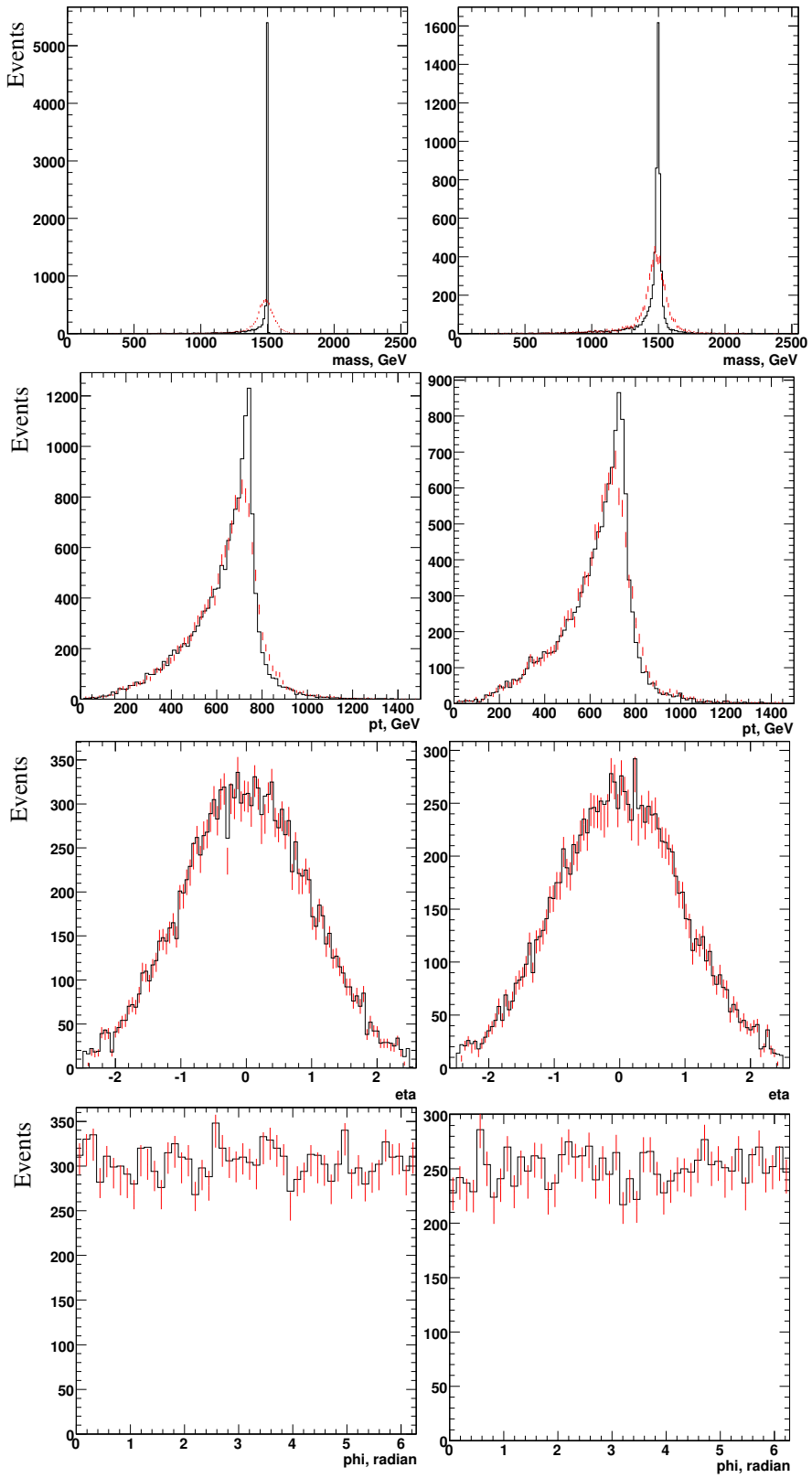

Figure 6: Examples of reconstruction of various kinematical distributions of muons (p_T, ϕ, η) from RS1-graviton decay for $M_{\rm grav} = 1500$ GeV with $c = 0.01$ (left-hand plots) and $c = 0.1$ (right-hand plots). The histograms are for the generated distributions, and the points with statistical uncertainties are for the reconstructed distributions.

4.1.1 Counting methods

To estimate the G_{KK} discovery limit one can use significance S_{cP} defined as probability from the Poisson distribution with mean N_B to observe greater or equal than $(N_S + N_B)$ events, converted to the equivalent number of sigmas of a Gaussian distribution [19], where N_S is the number of signal events passed through all kinematics cuts and N_B is the number of background events. This definition allows also to take into account statistical and systematic uncertainties of the background [19], for zero uncertainties it is close to the significance function S_{cL} suitable for small event samples [17] $S_{cL} = \sqrt{2((N_s + N_b)\ln(1 + N_s/N_b) - N_s)}$ which has been shown to give practically the same numerical values as S_{cP} estimator [19]. The distributions of various significance estimators show that these estimators are valid for both regions of small ($m = 1500$ GeV) and large ($m = 4000$ GeV) mass: the distribution for the case when a signal is present is Gaussian with the standard deviation close to 1, as well for the tail of the distribution for a case of only Drell-Yan background.

Since it is foreseen that in the real experiment the analysis of a found peak in the dimuon mass spectrum will be performed with fitting it with a hypothesis of Gaussian (or Gaussian-like) signal and an exponentially falling background, we obtain the numerical values of N_S and N_B from a similar fit also for the case of reconstructed Monte Carlo samples. The values of N_S and N_B are fixed according to the square under the corresponding fit curves in a 2σ window around the fitted peak value. Since the Drell-Yan mass spectrum is not exactly an exponential function, we use the sum of two exponentials (see Fig. 7)

$$f^{DY}(m) = \exp(a_1) \cdot \left[\exp\left(b_1 m + c_1 m^2\right) + \exp\left(a_2 + b_2 m + c_2 m^2\right)\right] \tag{2}$$

in a form which allows to vary the general background scale while fixing the shape of the distribution by releasing the first parameter a_1 and fixing the other ones. The values of the background parameters were obtained from fits to the full background only sample and fixed during the fit.

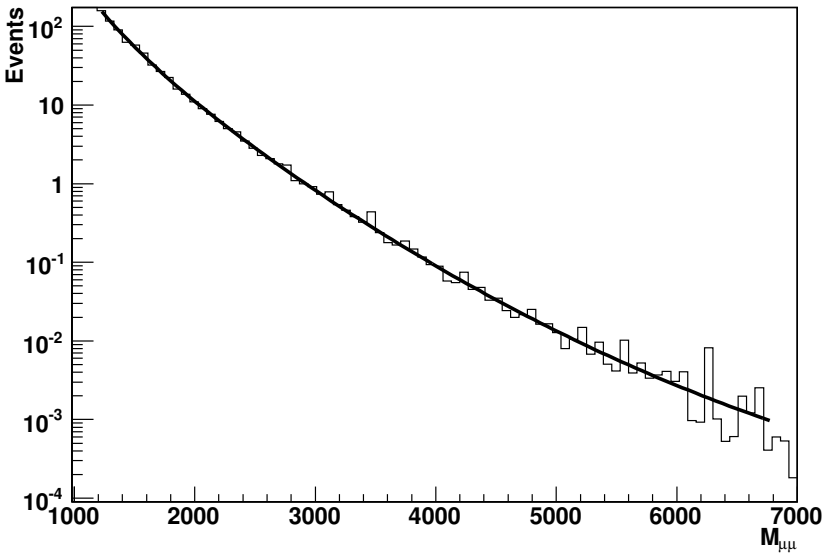

Figure 7: Reconstructed invariant mass distribution for the Drell-Yan background process, with the background-only fit Eq.(2) overlayed.

4.1.2 Likelihood fitting method

A procedure to estimate the CMS discovery reach has been set up following the approach outlined in [17] and applied in the nearly-identical case of Z' boson search in [18]. Signal observability was estimated by performing binned maximum-likelihood fits to reconstructed dimuon invariant mass spectrum and calculating the significance estimator

$$S_L = \sqrt{2\ln(\mathcal{L}_{s+b}/\mathcal{L}_b)} \tag{3}$$

where $\mathcal{L}_b$ and $\mathcal{L}_{s+b}$ are the best-fit likelihoods of the pdf's corresponding to the null hypothesis H_0 (no signal present) and the alternative hypothesis H_1 (signal plus background).

According to Wilks' theorem [20] in case of the absence of signal, the distribution of S_L^2 in the large statistics limit is a χ^2 with a number of degrees of freedom (ndof) equal to the difference in the number of free parameters in H_0 and H_1 pdf's. If the difference in ndof is equal to one, S_L is expected to follow a standard Gaussian distribution with the mean in 0 and a standard deviation of 1. This allows one to directly interpret the value of S_L as the significance level of the test, given as the commonly used "number of sigmas". That is, a S_L value of 5, often referred to as the "discovery limit" corresponds to a 2.9×10^{-7} probability that the signal is only a statistical fluctuation in the background (probability of a type-1 error).

The pdf used in the fit

$$p(M_{\mu\mu}; N_S, M_G, \Gamma, k) = N_S \cdot p_G(M_{\mu\mu}; M_G, \Gamma) + N_B \cdot p_{DY}(M_{\mu\mu}; k) \tag{4}$$

is a sum of signal and background pdf's, the background-only hypothesis is simulated by fixing $N_S = 0$.

The signal pdf p_G is a convolution of a negative Landau distribution modeling the radiative tail with a Gaussian accounting for the graviton width and mass reconstruction resolution (see Fig. 8):

$$p_G(M_{\mu\mu}; M_G, \Gamma) = Landau(-M_{\mu\mu}; -M_G, \tau) \otimes (r \cdot Gauss(M_{\mu\mu}; M_G, \Gamma_1) + (1-r) \cdot Gauss(M_{\mu\mu}; M_G, \Gamma_2)) \tag{5}$$

where:

- M_G is the mass of the resonance. In the fits it was fixed at a value obtained from a fit to the signal-only distribution.
- Γ_1 and Γ_2 are widths of the two Gaussians, accounting for the resonance width and muon momentum resolution tail. Currently they are also obtained from a fit to the full-statistics signal sample.
- r is the fraction of the two Gaussian parts.
- τ is the width of the Landau distribution modeling the radiative tail. Fits to generator-level pure signal samples have shown that a value of $0.006 \cdot M_G$ is a good approximation.

The background pdf is given as a sum of two exponents – see Eq.2. The values of the background pdf parameters were obtained from fits to the full background only sample and fixed during the fit. Other ways of determining these parameters were also explored and are discussed below. Including and omitting the quadratic term b was found to have a very small effect on the results of the fits, so the analysis was done with its value fixed at zero.

Toy Monte Carlo studies of the behavior of S_L, for a 1500 GeV graviton with coupling $c = 0.01$, for many simulated pseudo-experiments are shown in Fig. 9. Plots for other choices of Randall-Sundrum model parameters are similar, in particular for all cases it can be noted that:

- The tail of the distribution for a case with no signal is consistent with a standard Gaussian.
- The distribution for the case when a signal is present is also Gaussian, with the standard deviation close to 1 and mean within 5% of the S_L value obtained from fits to the full MC samples.

This confirms the validity of using S_L to estimate signal significance.

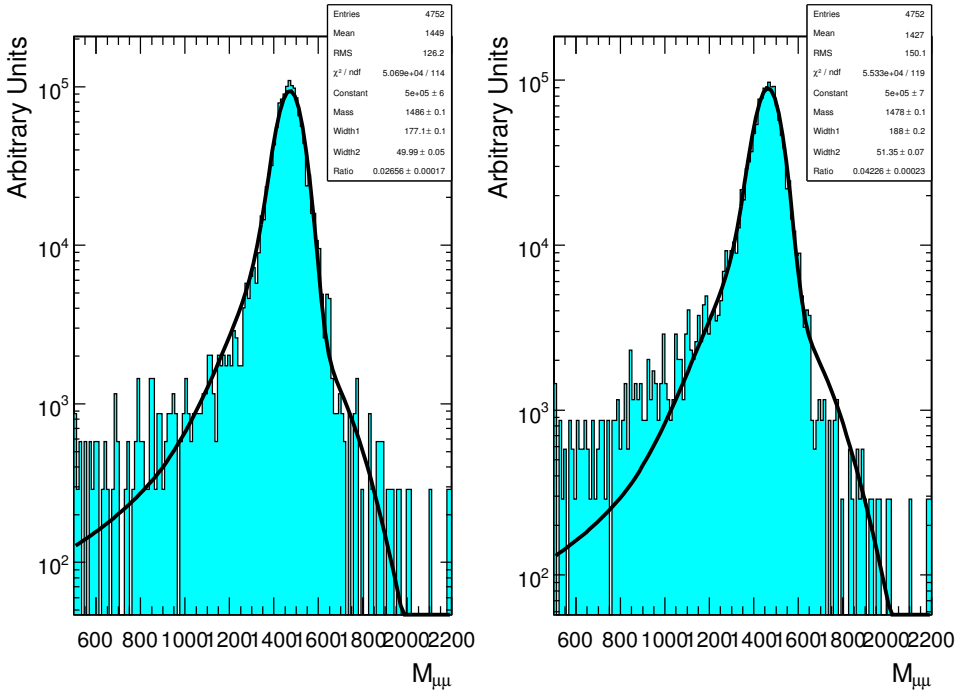

Figure 8: Reconstructed invariant mass distribution for a pure signal sample, with the signal pdf fit overlayed. A graviton with mass 1.5 TeV and $c = 0.01$ is plotted, the normalisation is arbitrary. The left plot shows the distribution with the bremsstrahlung photon correction included, the right plot shows the distribution without it.

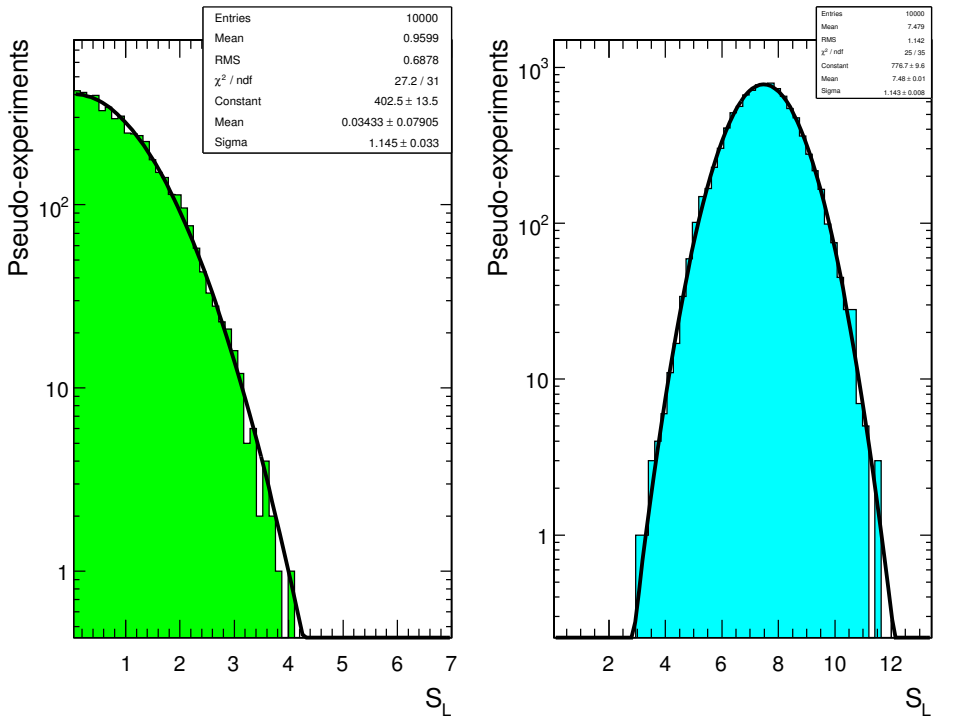

Figure 9: Distributions of S_L values obtained in fits to 10000 simulated pseudo-experiments for integrated luminosity of $100\,\text{fb}^{-1}$. The case when only the Drell-Yan background was present is shown on the left plot, the right plot shows the results for a 1500 GeV graviton. The curves represent Gaussian fits to the histograms.

4.1.3 Results for CMS Discovery Limit

Fig. 10 displays curves of the CMS mass reach as a function of integrated luminosity required for a five σ discovery. Here the four curves for the RS1 model parameter $c = 0.01$, 0.02, 0.05 and 0.1 (from top to bottom) are presented. The results for the different values of an integrated luminosity are summarized in Table 6. The CMS experiment allows to observe the RS1 graviton with mass up to 2.3 TeV using the first LHC data at $\int L\,dt = 1$ fb^{-1} if c is equal to 0.1. For $c = 0.01$ the mass reach is not more than 2 TeV even for asymptotic regime of LHC operation with $\int L\,dt = 300$ fb^{-1}. The asymptotic reach limit for $c = 0.1$ is 4.5 TeV.

Table 6: The dimuon mass reach (in TeV) for the CMS discovery potential to observe the RS1 graviton in $\mu^+\mu^-$ channel (statistical uncertainties only).

Coupling constant c	Estimator	1 fb^{-1}	10 fb^{-1}	100 fb^{-1}	300 fb^{-1}
0.01	S_{cP}	0.75	1.20	1.69	1.95
	S_{cL}	0.77	1.21	1.71	1.97
	S_L	0.78	1.23	1.73	1.99
0.02	S_{cP}	1.21	1.72	2.30	2.63
	S_{cL}	1.22	1.72	2.31	2.64
	S_L	1.22	1.74	2.34	2.68
0.05	S_{cP}	1.83	2.48	3.24	3.67
	S_{cL}	1.85	2.49	3.26	3.71
	S_L	1.85	2.51	3.31	3.79
0.1	S_{cP}	2.34	3.11	4.12	4.52
	S_{cL}	2.36	3.13	4.14	4.54
	S_L	2.36	3.16	4.23	4.73

A combined analysis [12] of the RS1 scenario shows that the value of the dimensionless coupling constant c is strongly restricted (Fig. 11) due the theoretical constraints to assure that the model does not introduce a new hierarchy (the scale parameter $\Lambda_\pi = M_{Pl}e^{kr_c\pi} < 10$ TeV). Fig. 11 shows that a luminosity of 100 fb^{-1} is sufficient to test the RS1 model everywhere in (c – $M_{\rm grav}$) space of model parameters. These conclusions, however, are not definitive, since initial theoretical constraints are quite arbitrary.

The previous studies of the potential of the CMS experiment to detect a RS1 graviton in the di-muon channel were based on the fast simulation program and give the following results for $\int Ldt$ = 100 fb^{-1}:

- The Notes [8, 9] shown that RS1 scenario can be probed at 95 % exclusion limit up to 1.7 TeV and 3.9 TeV for $c = 0.01$ and 0.1, respectively. Signal and background events were selected inside $\pm 2\Gamma_{\rm obs}$ the mass around the RS1 mass, where $\Gamma_{\rm obs}$ is defined as the observed width of the resonance state after smearing due to the detector effects.
- In the analysis described in Ref. [10] the CMS potential to discover the RS1 graviton with the 5σ significance is estimated at the level of 2.6 TeV for $c = 0.01$ and 4.8 TeV for $c = 0.1$. This analysis was done in assumption of a Gaussian behaviour of events and using the $S/\sqrt{B}$ estimator of the significance. To ensure the statistical significance of the signal for low background the minimal number of signal events, $S_{\rm min}$, equal to ten has been required, i.e. $S_{\rm min} = \max(5\sqrt{B}, 10)$. Instead of the $\pm 2\Gamma_{\rm obs}$ window the selection criteria $\pm 3\Gamma_{\rm obs}$ was used.

The difference between the current results and previous one can be explained by difference in statistical methods used for analyses, differences in reconstruction and selection efficiency (in the pioneering work only acceptance inefficiency was taken into account while the current study is based on the knowledge of the overall inefficiency including acceptance, trigger and off-line reconstruction inefficiency).

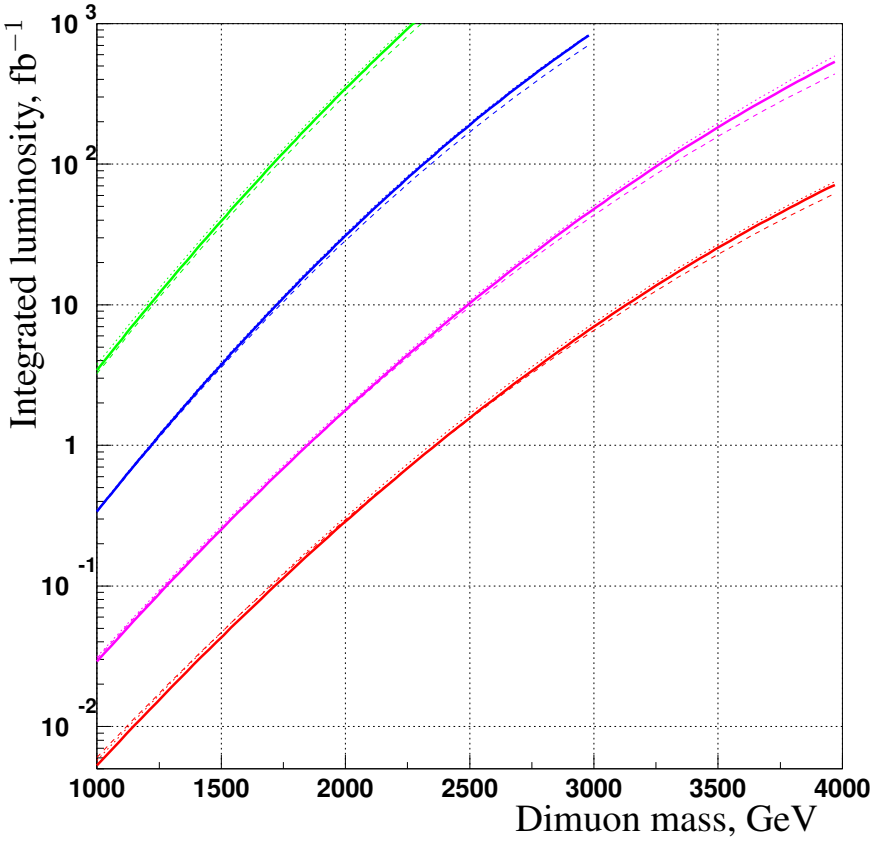

Figure 10: Discovery limit for RS1 graviton in the $\mu^+\mu^-$ decay mode for different values of RS1 coupling constant $c = 0.01$, 0.02, 0.05, 0.1 (the curves from top to bottom). Used discovery limit $S > 5$ for three significance estimators S_{cP} (solid lines), S_{cL} (dotted lines) and S_L (dashed lines).

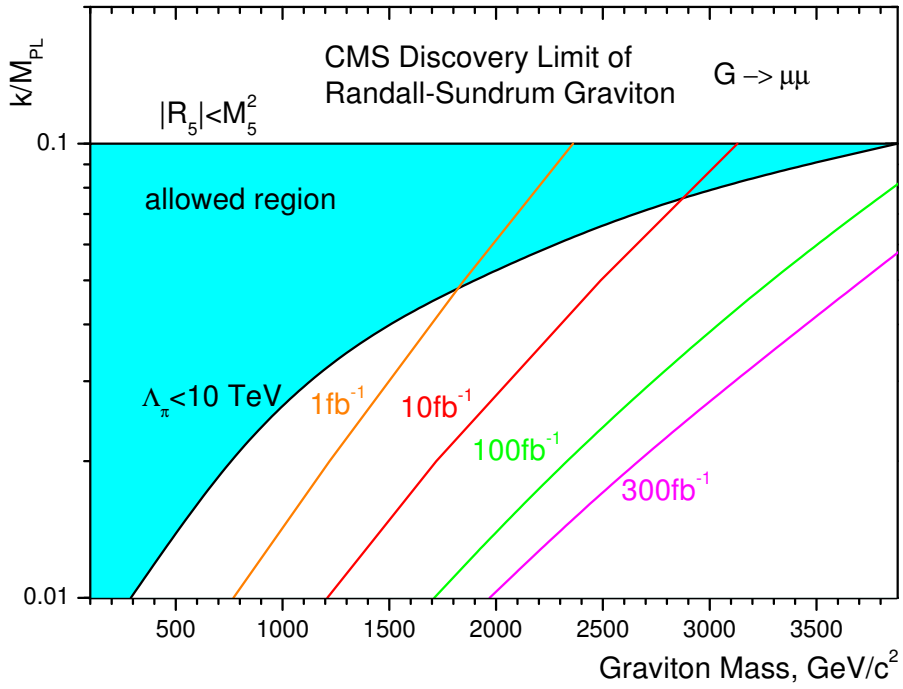

Figure 11: Theoretical and experimental constraints on the RS1 scenario parameter in the k/M_{Pl} and $m_1 = m_{G^\star}$ plane

5 Distinguishing between a graviton and a Z'

Once a new resonance has been discovered, its properties have to be determined, in order to establish its identity. A characteristic feature of the graviton is its spin-2 nature. Other particles usually considered which give a similar signature are spin-1 Z' extra gauge bosons [18]. The spin of the observed resonance manifests itself in the angular distributions of its decay products (see also Fig. 12):

subprocess	angular distribution
$q\bar{q} \to \gamma/Z^0/Z' \to f\bar{f}$	$\frac{3}{8}(1+\cos\theta^{*2})$
$q\bar{q} \to G^* \to f\bar{f}$	$\frac{5}{8}(1-3\cos\theta^{*2}+4\cos\theta^{*4})$
$gg \to G^* \to f\bar{f}$	$\frac{5}{8}(1-\cos\theta^{*4})$

where $\cos\theta^*$ is the angle between the incident quark or gluon and the outgoing lepton in the dimuon center-of-mass frame. In an experimental situation the transverse momenta of the incoming parton directions are not known, in such a case optimal results are achieved by calculating $\cos\theta^*$ in the Collins-Soper frame [21]. In order to reduce the contamination from the Drell-Yan background, only events in a $\sim 2\sigma$ mass window around the resonance peak are considered in this analysis.

The problem of determining the spin of the observed particle is, as in the case of the mass reach, a problem of rejecting one spin hypothesis H_0, thus accepting the alternative H_1. [1)] In a search for a Randall-Sundrum graviton, one is tempted to treat spin-1 as the null "background-only" hypothesis and repeat the reasoning from Section 4.1.2 with angular distributions in the place of invariant mass spectra. This approach is, however, asymmetric in the treatment of the two hypotheses: spin-1 exclusion with a given significance level, claimed on the basis of this test, will only happen in a real experiment with a 50% chance. In other words, the probability of a type-2 error (rejecting H_1 when it is true) of such a test is 50%. This is so by construction, since the significance level S_L is the **mean** of the distribution of the expected values of this test statistic.

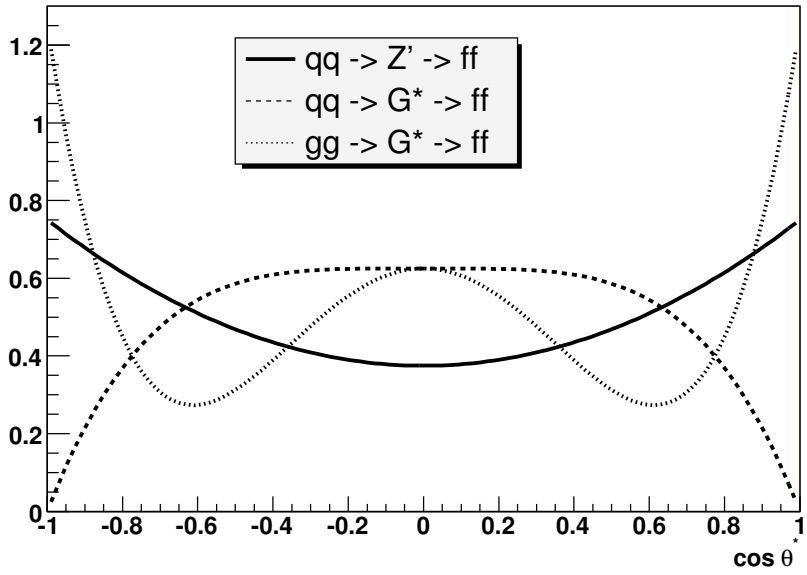

Figure 12: Angular distribution shapes for spin-1 and spin-2 resonances.

In order to treat the two hypotheses on a more equal footing, following [22] we construct a test with equal probabilities of type-1 and type-2 errors. In a case when the S_L distribution is Gaussian for both H_0 and H_1 (with means m_0, m_1 and sigmas σ_0, σ_1 respectively), this corresponds to finding x such that

$$m_0 + x \cdot \sigma_0 = m_1 - x \cdot \sigma_1 \ .$$

[1)] This is of course true only in a two hypotheses case. Since most current theoretical predictions for a very massive di-lepton resonance are spin-1 or spin-2 particles, other options (for example spin-0) are not considered here.

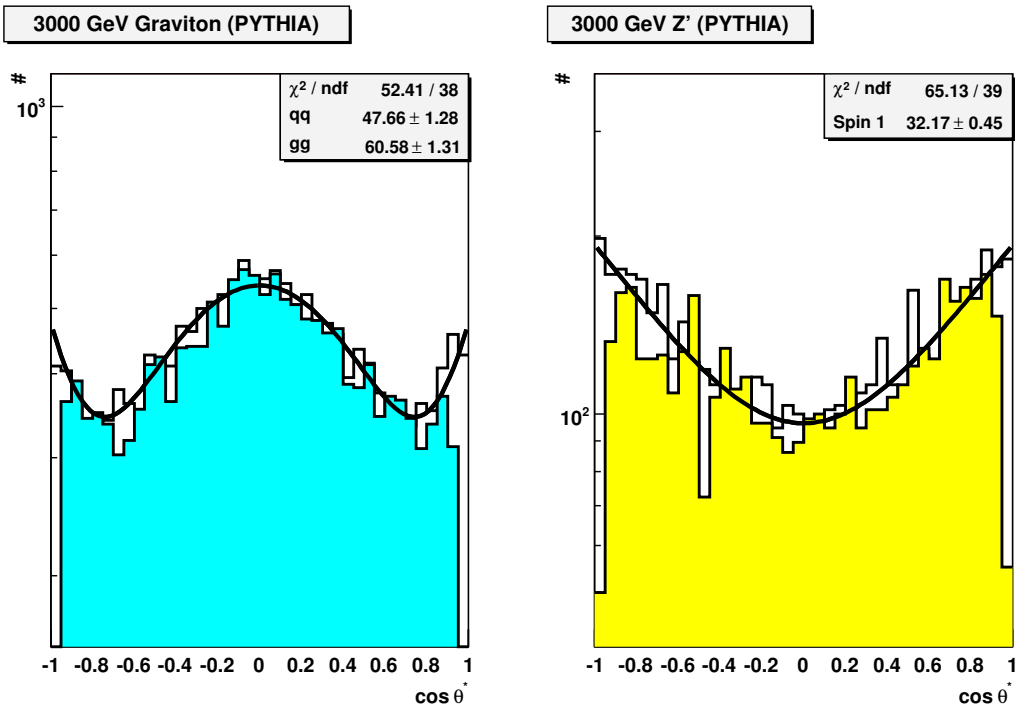

Figure 13: Angular distributions for 3000 GeV generated Z' (right) and graviton (left). Open histograms correspond to generator-level data, while the coloured histograms show events after full detector simulation and reconstruction. Theoretical curves fit to the Monte Carlo data are overlayed.

Note that this reasoning does not affect the interpretation of S_L once data is in hand, it only applies to quantifying the expected sensitivity of a planned experiment. Real data will give a certain value of our test statistic, and it can/will be converted to the significance level.

The analysis closely follows the method described in [22], where an unbinned likelihood is calculated for the graviton and Z', under the two hypotheses considered. The ratio of the $q\bar{q}$ and gg graviton production processes and signal-to-background ratio for the graviton are fixed, so there are no free parameters. The test statistic used to distinguish the two hypotheses is the likelihood ratio:

$$-2\ln\lambda = 2\ln\mathcal{L}_1 - 2\ln\mathcal{L}_2 \ . \tag{6}$$

In a case with no free parameters this is simply a sum of contributions from all the observed events. Fig. 14 shows these contributions for the full sample of signal and background events reconstructed in the mass window, for a 1000 GeV graviton and Z'. A real experiment corresponds to selecting the appropriate number of events N from this distribution and adding the contributions. In such a case, the Central Limit Theorem implies that the value of $-2\ln\lambda$ should follow a Gaussian distribution with mean and sigma calculated by scaling the mean and RMS values of the histograms in Fig. 14 by N and $\sqrt{N}$, respectively. This is indeed so, an example plot for 1000 GeV resonance mass is shown in Fig. 15. The significance level can be calculated for each set of simulated model parameters, either by running toy Monte Carlo taking the means and widths of the Gaussians for H_1 and H_2 from fits to the distributions of $-2\ln\lambda$, or by simply rescaling the mean and RMS of histograms with all reconstructed events in the mass window. The results agree within 5%, and so latter method was used. The CMS reach in the $M_G - k/M_{Pl}$ plane is shown for different values of integrated luminosity in Fig. 16 and summarized in Table 7.

Table 7: The CMS mass reach for distinguishing the RS1 graviton and spin-1 states at 2σ level (in GeV).

Integrated luminosity	10 fb^{-1}	100 fb^{-1}	300 fb^{-1}
$c = 0.01$	843	1128	1264
$c = 0.1$	1946	2524	3000

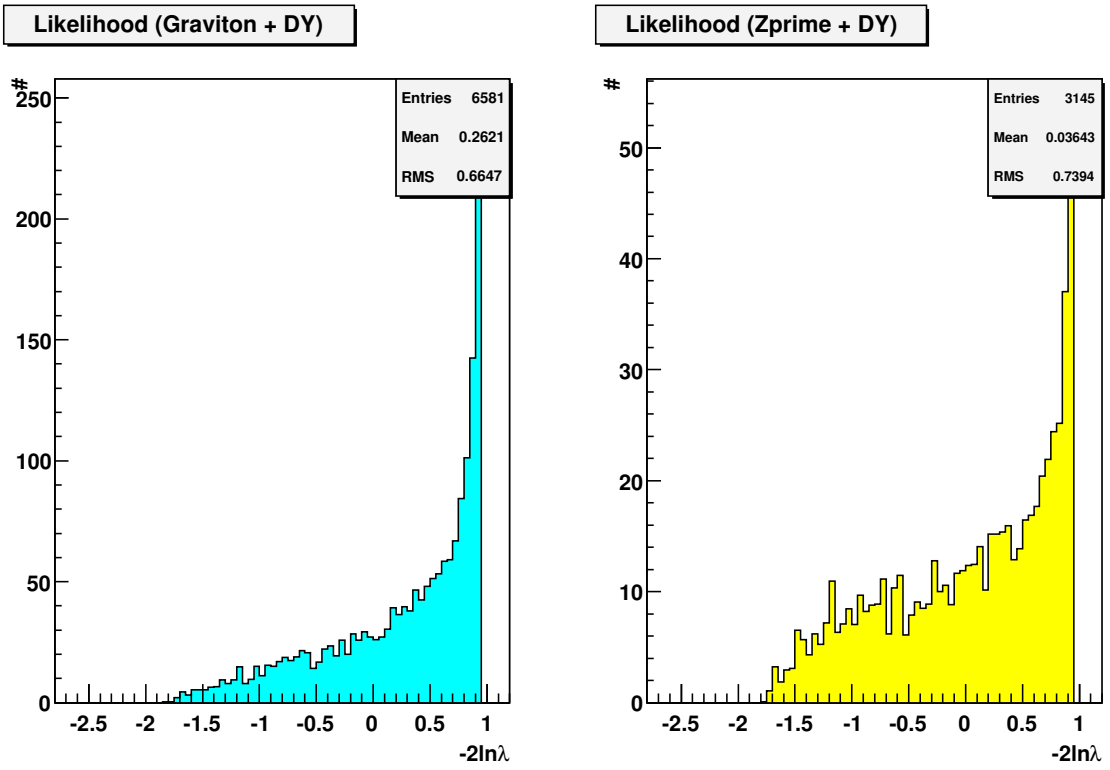

Figure 14: Contributions to the likelihood function (Eq. 6) from individual simulated events, for a 1000 GeV Z' (right) and graviton (left), with the Drell-Yan contribution added.

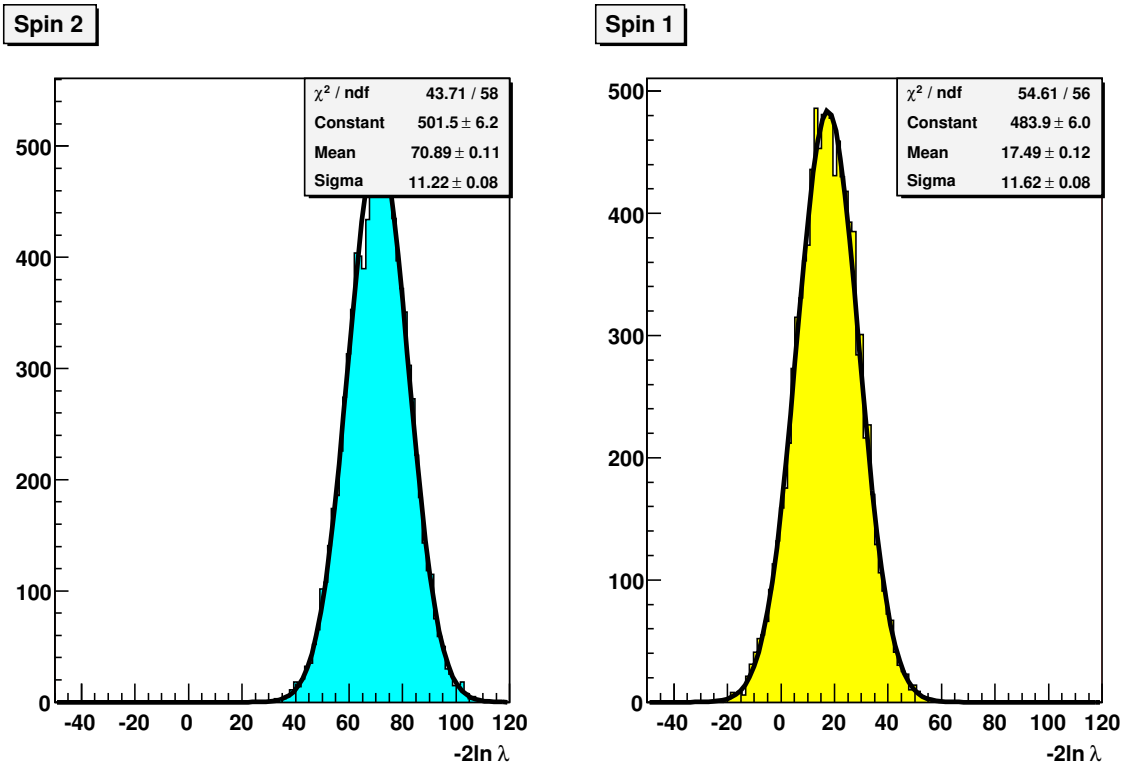

Figure 15: Values of $-2\ln\lambda$ obtained in 10000 pseudo-experiments, for a 1000 GeV Z' (right) and graviton (left).

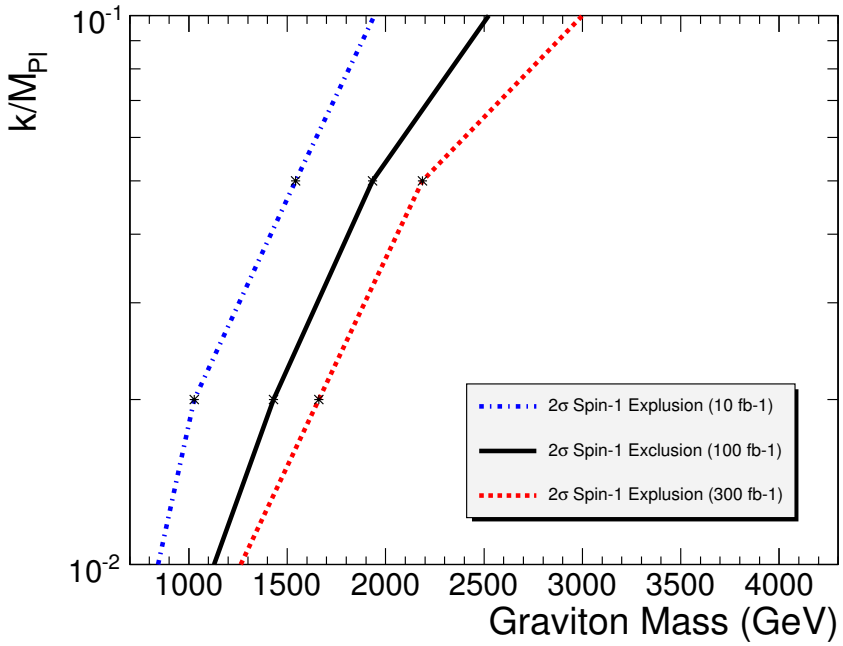

Figure 16: CMS reach for 2σ discrimination between spin-1 and spin-2 hypotheses for different integrated luminosities.

6 Systematic uncertainties and treatment of real data

The above results were obtained assuming a perfectly aligned detector, precise knowledge of the detector performance and ideal Monte Carlo. In this section we will relax the various assumptions made in the analysis and check how this affects the final result.

6.1 Sources of systematic uncertainty

To extract correctly the signal events from the background we should understand the reliability of the calculations of dilepton spectrum within the Standard Model to keep under control all possible sources of errors and systematic uncertainties. These systematics can be related to a) the accuracy of the theoretical calculations, b) the accuracy of the phenomenological determination of PDF's and c) the experimental uncertainties – detector resolution, goodness of fits etc. The main of them are:

- **The QCD and EW radiative corrections.** A possible theoretical ambiguity in such studies is induced by incomplete accounting of contributions from QCD and electroweak higher-order quantum corrections to the considered processes. As it was mentioned before, the current calculations of RS1 and Drell-Yan cross section were done in the leading order for the CTEQ6M with the K-factor of 1.0. To take the systematic uncertainty of the K-factor in the present study, we use the value of $K = 1.30 \pm 0.05$. It is also expected that the electroweak NLO corrections are of the order of 10 % [23]. The uncertainties of the hard process scale [24] give the following modification of the results: for RS1 signal about 11–17% variation and for DY background about 3–12% (the former numbers correspond to 1 TeV dimuon mass, and the latter ones to 5 TeV).

- **PDF-related uncertainties.** The phenomenological origin of the PDFs gives one another systematic error. First of all, the cross section values obtained using different sets of structure functions are not quite equal. These results are varying within ± 7 % for $M_{ll} \geq 1$ TeV.

  In addition, there are uncertainties within the bounds of the same set (so called *internal* uncertainties) coming from an accuracy of the global analysis of experimental data and from experimental measurement errors. A recently developed PDF building technique goes beyond the "standard" extraction of only one "best fit". Last versions of PDF contain a set of various alternative fits obtained by subjective tuning of specific degrees of freedom for this PDF [25]. Applying standard statistical methods one can analyze internal uncertainties

Table 8: The modification of summary results for CMS discovery potential invariant mass reach (in TeV) for various misalignment scenarios and significance estimator S_{cL}.

Coupling constant c	Scenario	1 fb^{-1}	10 fb^{-1}	100 fb^{-1}	300 fb^{-1}
0.01	No misalignment	0.77	1.21	1.71	1.97
	Long Term	0.74	1.18	1.65	1.92
0.1	No misalignment	2.36	3.13	4.15	4.54
	Long Term	2.34	3.09	4.03	4.43
	First Data	2.03	—	—	—

using the master equation [24]

$$\Delta X_C = \frac{1}{2}\sqrt{\sum_{k=1}^{2d}(X_k - X_0)^2}\ ,$$

where X_0 is the cross section evaluated with the "best-fit" PDF (CTEQ6m) and X_k is the cross section evaluated with the k-th PDF subset. The obtained uncertainties are about 10–46% for the RS1 signal and about 3–18% for the DY background (the former numbers correspond to 1.5 TeV dimuon mass and the latter ones to 5 TeV).

- **Misalignment.** There are two scenarios of misalignment of the Muon detector and Tracker for usage in the CMS PRS studies: "First Data" scenario corresponding to the initial period of alignment (up to approximately 1 fb^{-1} integrated luminosity), and "Long Term" scenario corresponding the nominal CMS operation (see details in [26]). The full simulation of the misalignment process in ORCA [15] for the RS1 events shows an increase of the dimuon mass residuals by around 30% for the long term misalignment and by a factor around 3–4 for the first data misalignment (see Fig. 17). The corresponding modification of the required integrated luminosity as a function of graviton mass for 5σ discovery is demonstrated in Fig. 18. The required CMS invariant mass reach for various misalignment scenarios is shown in Table 8. One can see that induced misalignment effects lead to decreasing the CMS discovery potential invariant mass reach by up to 0.1 TeV for the Long Term misalignment scenario and a substantially worse degradation for the First Data scenario.

- **Pile-up.** The results in Section 4.1.3 were obtained using events simulated without pile-up of minimum-bias collisions (corresponding to the conditions of the initial data taking). Simulation with pile-up corresponding to the high-luminosity scenario with 25 collisions per bunch crossing at $\mathcal{L} = 10^{34}$ cm^{-2}s^{-1} shows that the widths of dimuon mass residuals increase by around $0.1 - 0.2\%$ (compared to $3 - 5\%$ without pile-up), therefore the whole effect is much smaller than the influence of the misalignment for the Long Term scenario.

- **Magnetic field uncertainty** in the muon chambers can cause a scale shift in the dimuon mass resolution by 5–10% [27]. But since magnetic field uncertainty in the tracker is expected to be small (Ref. [28] quotes 0.03%), the uncertainty in the muon chambers should give only a small impact for the overall dimuon mass determination. Besides, if we choose 3% scale uncertainty [27], that will shift the mass equally for signal and background, and the significance will not change much, but the mass measured in the peak will move. So the corresponding shifts in the mass reach values are negligible.

- **Variations of the background shape** in the fits produce a drop of about 10–15% in the significance values. The possible variations of the background shape were studied by applying an additional factor $\exp(\alpha(m - m_0))$ in the fit with an additional free parameter α to the function Eq.(2) describing the Drell-Yan Background with fixed coefficients a_2, b_i, c_i.

- **Trigger and reconstruction acceptance** uncertainties do not cause significant variations of the mass reach values since we fit the signal and background shape with a free normalization.

Taking these uncertainties into account, Fig. 19 displays curves of the CMS mass reach as a function of integrated luminosity required for a five σ discovery. The modified plot of theoretical and experimental constraints on the RS1 scenario parameter in the k/M_{Pl} and $m_1 = m_{G^\star}$ plane is shown in Fig.20.

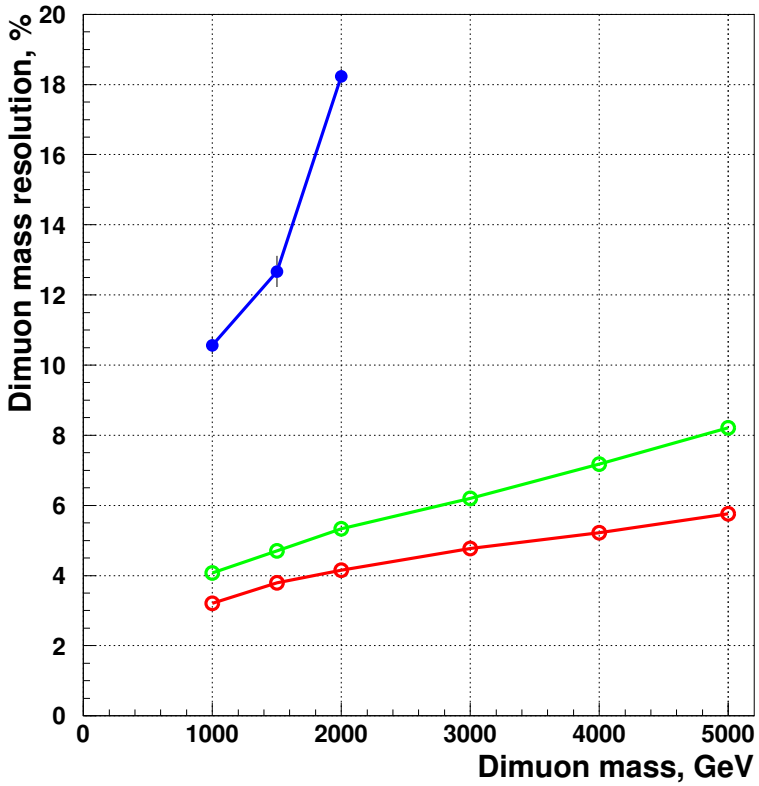

Figure 17: The influence of misalignment in various misalignment scenarios for the dimuon mass resolution. The curves (from bottom to top) correspond to the case of the ideal alignment, Long Term and First Data scenarios.

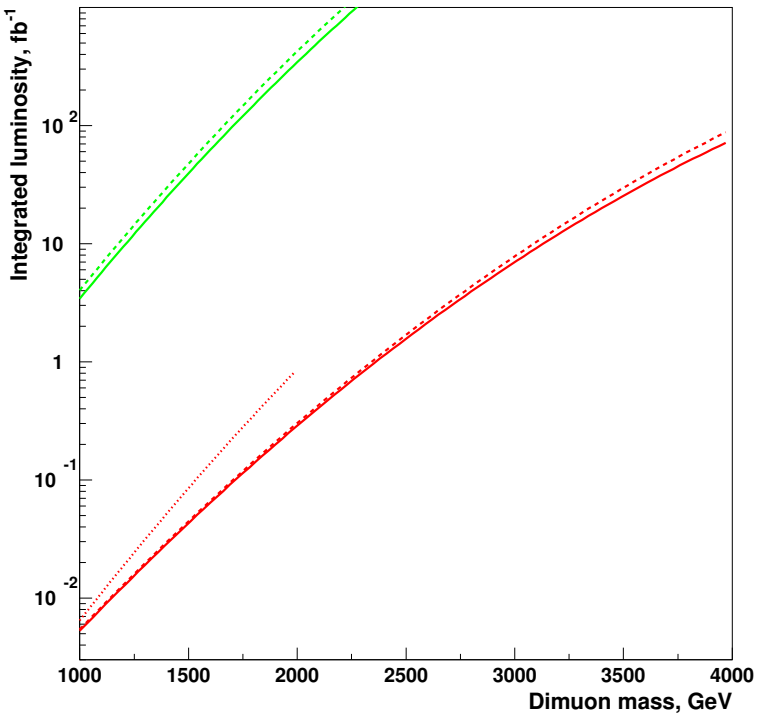

Figure 18: The influence of misalignment in various scenarios for the discovery limit for RS1 graviton with $\mu^+\mu^-$ decay mode for different values of RS1 coupling constant $c = 0.01$, 0.1 (the curves from top to bottom). The curves correspond to the case of the ideal alignment (solid lines), First Data scenario (dotted line) and Long Term scenario (dashed lines). Used discovery limit $S > 5$ for significance estimator S_{cL}.

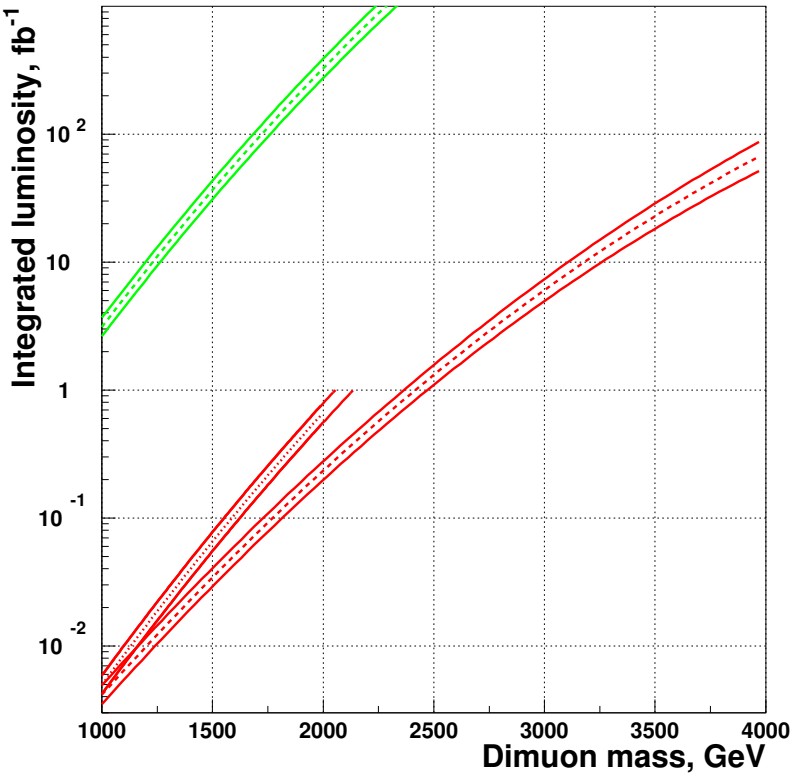

Figure 19: The influence of uncertainties for the discovery limit for RS1 graviton with $\mu^+\mu^-$ decay mode for different values of RS1 coupling constant $c = 0.01$, 0.1 (the curves from top to bottom). The upper curves correspond to the value of coupling constant $c = 0.01$, the lower ones to $c = 0.1$. The curves ending at integrated luminosity of 1 fb^{-1} correspond the First Data misalignment scenario, the other ones correspond to the Long Term scenario. The ranges show expected variations due to the systematic uncertainties.

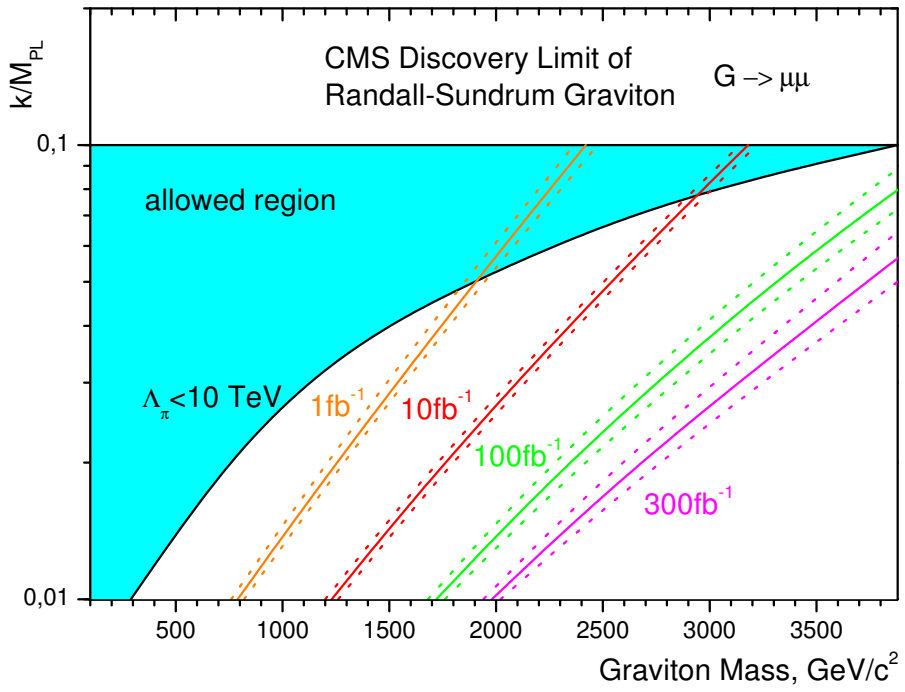

Figure 20: Theoretical and experimental constraints on the RS1 scenario parameter in the k/M_{Pl} and $m_1 = m_{G^\star}$ plane with the systematic uncertainties taken into account, for the First Data misalignment scenario.

6.2 Likelihood fitting estimators

In order to keep the difference in the number of free parameters between the signal+background and background only pdf's equal to one, the mass and width of the resonance were fixed in the fit. The logic behind this is different in each of the two cases: the mass of the new particle can be determined by "scanning" the Drell-Yan continuum with fits with different mass hypotheses (this is essentially equivalent to doing a fit with the mass as a free parameter). The value of M_G maximizing the signal likelihood corresponds to a hypothetical particle which is least probable to be a background fluctuation. The mass is then fixed at that value and the resulting S_L is interpreted as the significance level for rejecting H_0 and claiming the existence of a resonance with mass M_G, determined this way. The precision of the mass fit is illustrated on Fig. 21, where the values obtained in 1000 simulated pseudo-experiments are shown, along with a Gaussian fit to the distribution. Fig. 22 shows the distributions of the significance estimator for 1000 toy Monte Carlo experiments, in the case where the graviton mass in each pseudo-experiment is obtained as described above. No significant differences from the case with the mass fixed at the true value (Fig. 9) appear.

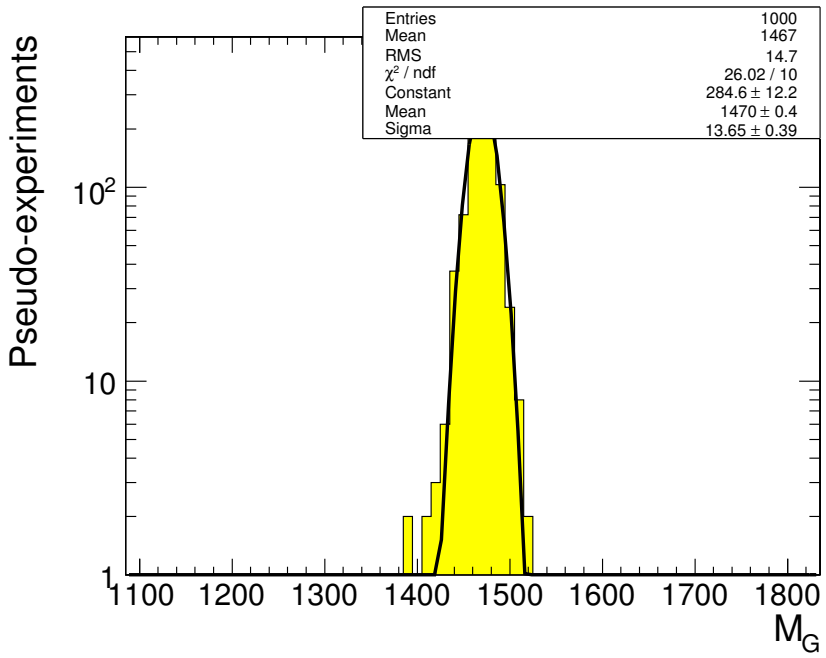

Figure 21: Reconstructed graviton mass distribution for a graviton with mass equal to 1500 GeV and $c = 0.01$. The plot shows results from 1000 toy Monte Carlo experiments, with a Gaussian fit overlayed.

The reason for fixing the resonance width is different – it is simply assumed to be known with sufficient precision. In the fit, there are two parameters governing the resonance width: the width of the Landau function and the FWHM of the Gaussian. The Landau function accounts mainly for the radiative tail, fixing the Landau width at zero affects only the mass fit – the mean reconstructed graviton mass is lower by $\sim$2% and the significance remains unchanged.

Fixing the parameters of the background pdf does not in principle affect the interpretation of S_L since this pdf appears in both H_0 and H_1 fits and the difference in the number of free parameters is not affected. Freeing the background parameters is however not a good choice since it makes the fit unstable and reduces the signal significance by $\sim 20\%$. In a real experiment it might be necessary to extract some or all of the background shape parameters from the data, depending on the level of relying on the Monte Carlo estimates. This is best done by fitting the background pdf in signal-free regions. The exact strategy depends on the graviton mass and on the amount of data available. For low-mass resonances (of the order of 1 TeV), the background can be approximated with a single exponent, and the slope can be obtained from a fit to the left sideband of the invariant mass spectrum. For large integrated luminosity, information can also be extracted from the region to the right of the resonance. For gravitons with masses above 2 TeV fits in the left sideband give a good approximation of the background parameters.

Such a procedure has the advantage of being largely independent of Monte Carlo simulation – if in reality the

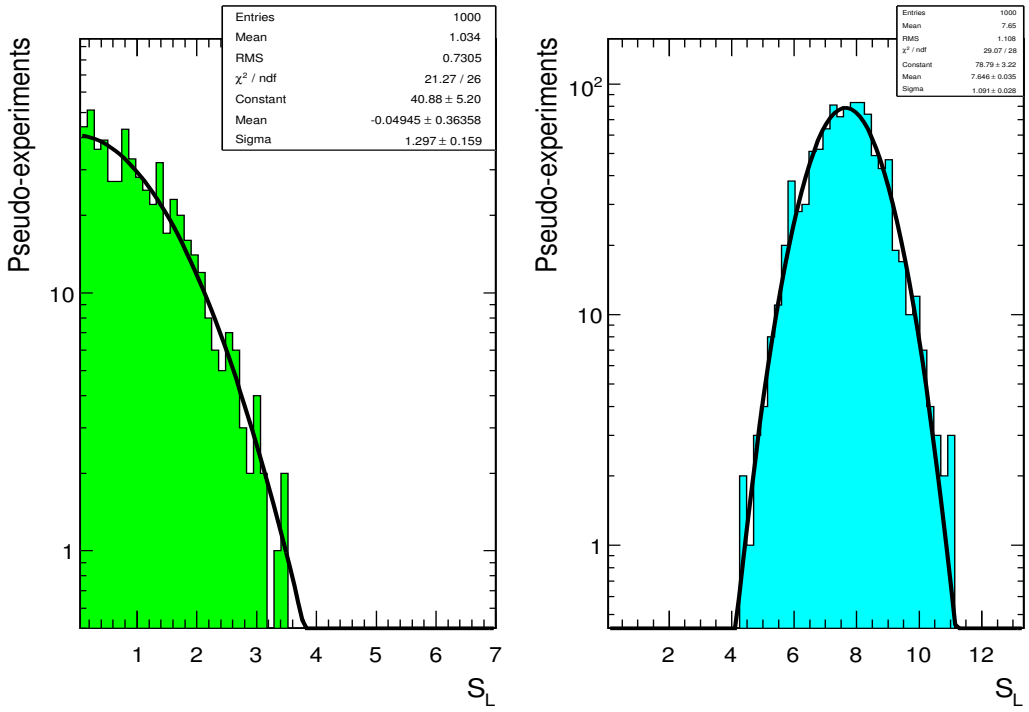

Figure 22: Distributions of S_L values obtained in fits to 1000 pseudo-experiments with $100 fb^{-1}$ integrated luminosity. In each pseudo-experiment the graviton mass was obtained by finding the value maximizing signal significance. The background only case is shown on the left plot, the right plot shows the results for a 1500 GeV graviton with $c = 0.01$. The curves represent Gaussian fits to the histograms.

background has a different slope or normalization than assumed in the present analysis, the results will be different, but will remain valid. The price to pay for this is a $\sim 10\%$ reduction in signal significance (with respect to the ideal case where background shape is taken from MC) and additional statistical uncertainty – the FWHM of the S_L distribution changes to a value of ~ 1.5, from ~ 1 in the ideal case.

7 Summary

In this work, the study of Randall-Sundrum graviton decay into muon pairs has been performed. A full simulation and reconstruction analysis was carried out to derive both the CMS discovery potential for Randall-Sundrum graviton and spin determination in this channel. Systematic uncertainties are taken into account. These results are summarized in Fig. 19, where the two mass reach limit curves as a function of integrated luminosity are presented for the coupling constant $c = 0.01$ and $c = 0.1$. About 1–2 TeV mass region is available for exploration during the LHC startup run with $\int Ldt$ = 1 fb^{-1}. For higher statistics, $\int Ldt$ = 100 fb^{-1}, a RS1 graviton can be observed with a 5σ limit up to the mass values of 1.7 TeV for $c = 0.01$ and 4.1 TeV for $c = 0.1$. And finally, the asymptotic regime of LHC operation $\int Ldt$ = 300 fb^{-1} allows to extend these limits up to 1.9 TeV and 4.5 TeV, respectively. For an integrated luminosity of $\int Ldt$ = 100 fb^{-1}, the spin-1 and spin-2 hypotheses can be discriminated at 2σ level for gravitons with mass up to 1.1 TeV for $c = 0.01$ and 2.5 TeV for $c = 0.1$.

Acknowledgments

We would like to thank D. Acosta, D. Bardin, S. Bityukov, R. Cousins, A. De Roeck, A. Nikitenko, M. Spiropulu, L. Pape and V. Valuev for interesting discussions and I. Antoniadis and V. Rubakov for helpful discussions on different scenarios. I.B. acknowledges the financial support provided by the INTAS program.

References

[1] D0 Collaboration, B. Abbott et al. "Measurement of the high mass Drell-Yan cross-section and limits on quark electron compositeness scales", *Phys. Rev. Lett.* **82** (1999) 4769.

[2] OPAL Collaboration, K. Ackerstaff et al., "Production of fermion pair events in e+e- collision at 161-GeV center-of-mass energy", *Phys. Lett.* **B391** (1997) 221.

[3] N. Arkani-Hamed, S. Dimopoulos and G. Dvali, "The Hierarchy Problem and New Dimensions at a Millimeter", *Phys. Lett.* **B429** (1998) 263; I. Antoniadis, N. Arkani-Hamed, S. Dimopoulos and G. Dvali, "New Dimensions at a Millimeter to a Fermi and Superstrings at a TeV", *Phys. Lett.* **B436** (1998) 257.
Phenomenology and astrophysics limits of the model can be found in
N. Arkani-Hamed, S. Dimopoulos and G. Dvali, "Phenomenology, Astrophysics and Cosmology of Theories with Sub-Millimeter Dimensions and TeV Scale Quantum Gravity", *Phys. Rev.* **D59** (1999) 086004.
Superstring realization of the model can be found in
D. Cremades, L.E. Ibanez and F. Marchesano, "Standard Model at Intersecting D5-branes: Lowering the String Scale", *Nucl. Phys.* **B643** (2002) 93; C. Kokorelis, "Exact Standard model Structures from Intersecting D5-Branes", *Nucl. Phys.* **677** (2004) 115.

[4] L. Randall and R. Sundrum, "A large mass hierarchy from a small extra dimension", *Phys. Rev. Lett.* **83** (1999) 3370; "An alternative to compactification", *Phys. Rev. Lett.* **83** (1999) 4690.

[5] V.A. Rubakov, "Large and infinite extra dimensions", *Usp. fiz. nauk* **171** (2001) 913 (in Russian); *Phys. Usp.* **44** (2001) 871, hep-ph/0104152 (English version).

[6] D.I. Kazakov, "Beyond the Standard Model" [hep-ph/0411064].

[7] I. Antoniadis, "A Possible New Dimension at a few TeV", *Phys. Lett.* **B246** (1990) 377;
I. Antoniadis and K. Benakli, "Limits on Extra Dimensions in Orbifold Compactifications of Superstrings", *Phys. Lett.* **B326** (1994) 69;
I. Antoniadis, K. Benakli and M. Quiros, "Production of Kaluza-Klein States at Future Colliders", *Phys. Lett.* **B331** (1994) 313.

[8] C. Collard, M.-C. Lemaire, P. Traczyk and G. Wrochna, "Prospects for Study of Randall-Sundrum Gravitons in the CMS Experiment", CMS Note 2002/050.

[9] P. Traczyk and G. Wrochna, "Search for Randall-Sundrum Graviton Excitations in the CMS Experiment", hep-ex/0207061.

[10] I. Golutvin, P. Moissenz, V. Palichik, M. Savina and S. Shmatov, "Search for TeV Scale Bosons in the Dimuon Channel With the CMS Detector", *Czech. J. Phys.* **64** (2004) A261, CMS CR-2004/026 [hep-ph/0310336].

[11] C. Collard and M.-Cl. Lemaire, "Search with the CMS Detector for Randall-Sundrum Excitations of Gravitons Decaying Into Electron Pairs", CMS Note 2004/024;
C. Collard, "Search for Randall-Sundrum Gravitons in CMS", Presented at: Physics at LHC, Vienna, 13-17 July, 2004, CMS CR-2004/036;
M.-C. Lemaire and J.-P. Pansart, "Search for Randall-Sundrum Graviton decaying into a pair of electrons and photons", CMS Note 2002/020.

[12] H. Davoudiasl, J.L. Hewett and T.G. Rizzo, "Experimental Probes of Localized Gravity: On and Off the Wall", *Phys. Rev.* **D63** (2001) 075004.

[13] T. Sjöstrand et al., "High-Energy Physics Event Generation with PYTHIA 6.1", *Comp. Phys. Commun.* **135** (2001) 238;
T. Sjöstrand et al., "PYTHIA 6.2 Physics and Manual", LUTP 01-21 [hep-ph/0108264].

[14] CMS Collaboration, CMS Simulation Package, version 3_6_5, `http://cmsdoc.cern.ch/oscar`

[15] CMS Collaboration, CMS Reconstruction Package, version 8_13_2, `http://cmsdoc.cern.ch/orca`

[16] I. Belotelov et al., "Study of Drell-Yan Dimuon Production with the CMS Detector", CMS Note 2006/123.

[17] V. Bartsch and G. Quast, "Expected Signal Observability at Future Experiments", CMS Note 2005/004.

[18] R. Cousins, J. Mumford and V. Valuev, "Detection of Z' Gauge Bosons in the Dimuon Decay Mode in CMS", CMS Note 2005/002.

[19] S.I. Bityukov, S.E. Erofeeva, N.V. Krasnikov, A.N. Nikitenko, "Program for evaluation of the significance, confidence intervals and limits by direct calculation of probabilities", Conference Proceedings of PHYSTAT2005: Statistical Problems in Particle Physics, Astrophysics and Cosmology, Editors: L. Lyons, M.K. Unel, Imperial College Press, 2006; `http://cmsdoc.cern.ch/~bityukov/`

[20] S. Wilks, "The Large-Sample Distribution of the Likelihood Ratio for Testing Composite Hypotheses", *Annals of Math. Stat.* **9** (1938) 60.

[21] J. Collins and D. Soper, "Angular Distribution of Dileptons in High-Energy Hadron Collisions", *Phys. Rev.* **D16** (1977) 2219.

[22] R. Cousins, J. Mumford, J. Tucker and V. Valuev, "Spin discrimination of new heavy resonances at the LHC", *JHEP* **0511** (2005) 046.

[23] U. Baur, O. Brein, W. Hollik, C. Schappacher and D. Wackeroth, "Electroweak Radiative Corrections to Neutral Current Drell-Yan Processes at Hadron Colliders", *Phys. Rev.* **D65** (2002) 033007;
V. Zykunov, "Weak Radiative Corrections to Drell-Yan Process for Large Invariant Mass of Di-Lepton Pair", hep-ph/0509315, to be published in Phys. Rev. D.

[24] P. Bartalini, R. Chierici and A. De Roeck, "Guidelines for the Estimation of Theoretical Uncertainties at the LHC", CMS Note 2005/013.

[25] M.R. Whalley, D. Bourilkov and R.C. Group, "The Les Houches Accord PDFs (LHAPDF) and LHAGLUE", hep-ph/0508110; `http://hepforge.cedar.ac.uk/lhapdf/`

[26] I. Belotelov et al., "Influence of Misalignment Scenarios on Muon reconstruction", CMS Note 2006/017;
I. Belotelov et al., "Simulation of Misalignment Scenarios for CMS Tracking Devices", CMS Note 2006/008.

[27] R. Cousins, J. Mumford and V. Valuev, "Detection of Z' Gauge Bosons in the Dimuon Decay Mode in CMS", CMS Note 2006/062.

[28] CMS Collaboration, "CMS Physics Technical Design Report, Vol. I: Detector Performance and Software", CERN/LHCC 2006-001, 2006.

A Plots for the dimuon mass spectra for RS1 model

In this appendix examples of plots for the dimuon mass spectra for RS1 model are shown for the values of RS1 graviton masses between 1 and 3 GeV and integrated luminosities between 0.01 and 100 fb^{-1}.

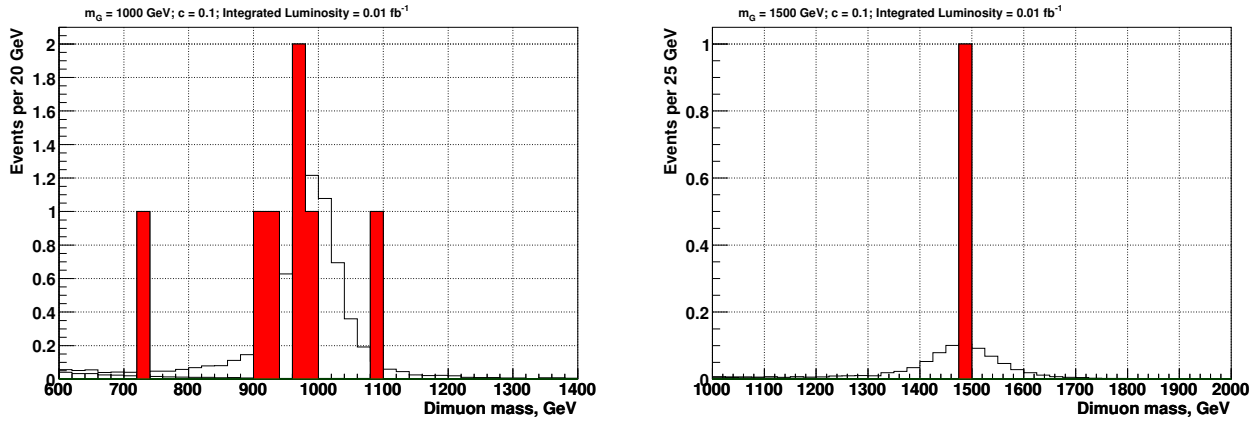

Figure 23: Reconstructed invariant mass distributions for RS1 graviton decaying into $\mu^+\mu^-$ pair. An example of Monte Carlo experiment is shown for integrated luminosity of 0.01 fb^{-1} and $c = 0.1$: the signal events are displayed for $m = 1000$ (left) and 1500 GeV (right). This example of Monte Carlo experiment does not contain background events. Curves show the limit of large statistics for the same integrated luminosity.

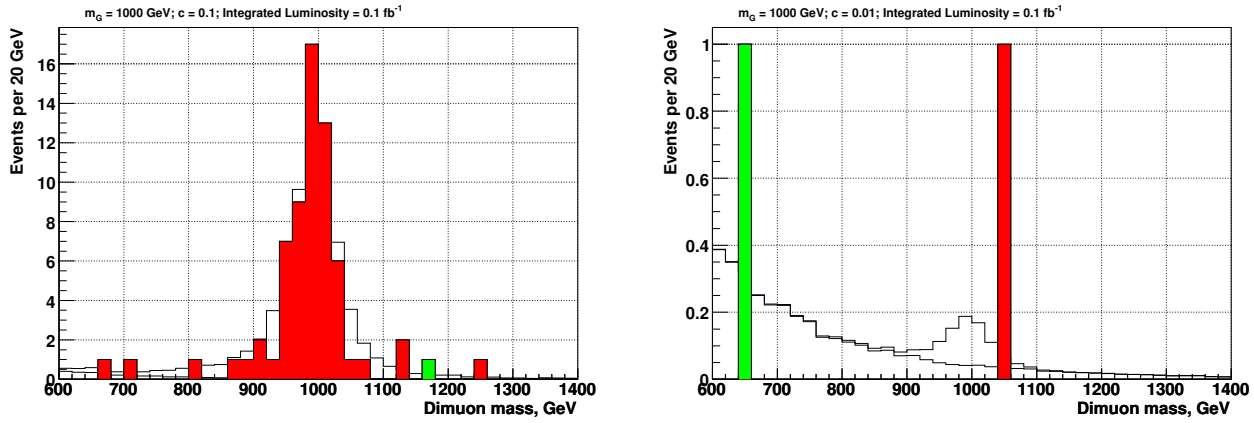

Figure 24: Reconstructed invariant mass distributions for RS1 graviton decaying into $\mu^+\mu^-$ pair. An example of Monte Carlo experiment is shown for integrated luminosity of 0.1 fb^{-1}: the signal (red dark area) is displayed over the background (green light area) for $m = 1000$ GeV. Left and right plots correspond to $c = 0.1$ and $c = 0.01$, respectively. Curves show the limit of large statistics for the same integrated luminosity.

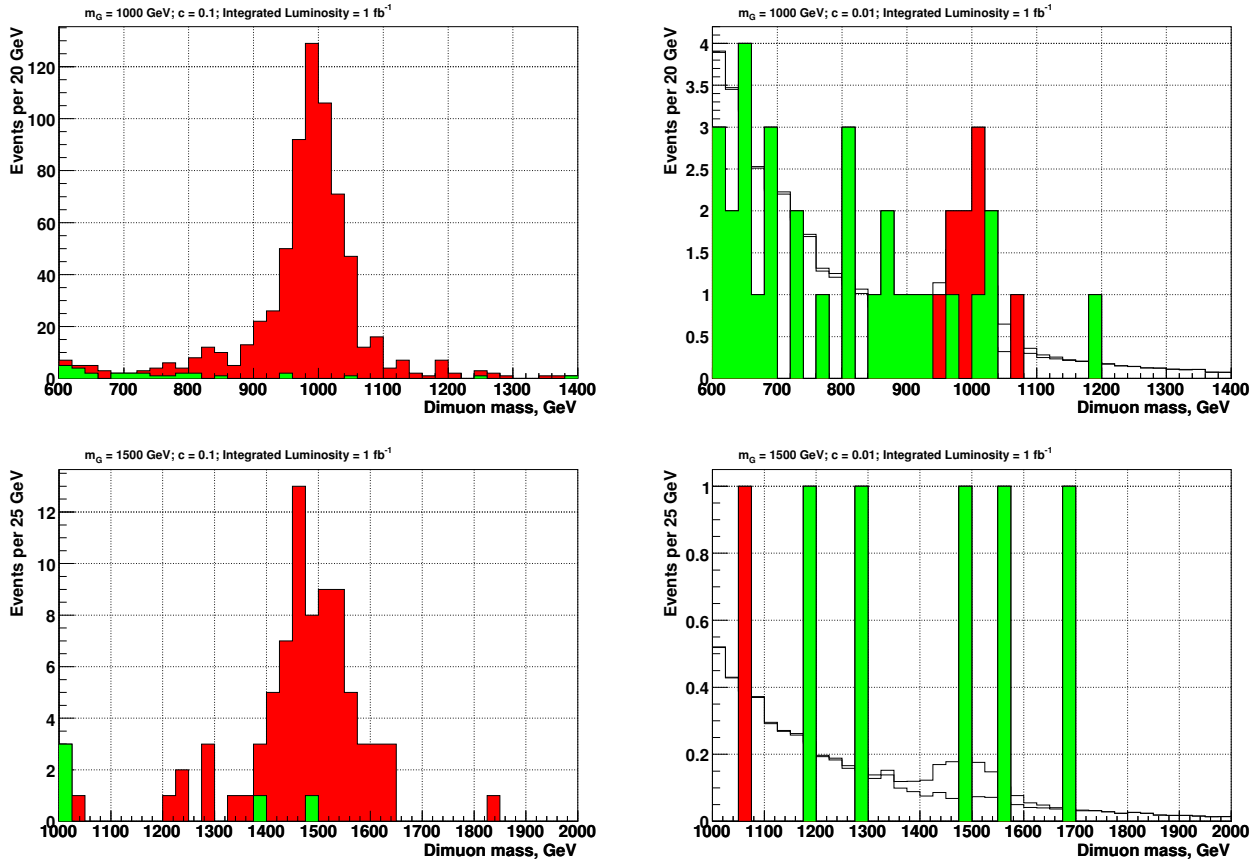

Figure 25: Reconstructed invariant mass distributions for RS1 graviton decaying into $\mu^+\mu^-$ pair. An example of Monte Carlo experiment is shown for integrated luminosity of 1 fb^{-1}: the signal (red dark area) is displayed over the background (green light area) for $m = 1000$ (top) and 1500 GeV (bottom). Left and right plots correspond to $c = 0.1$ and $c = 0.01$, respectively. Curves at the right plots show the limit of large statistics for the same integrated luminosity.

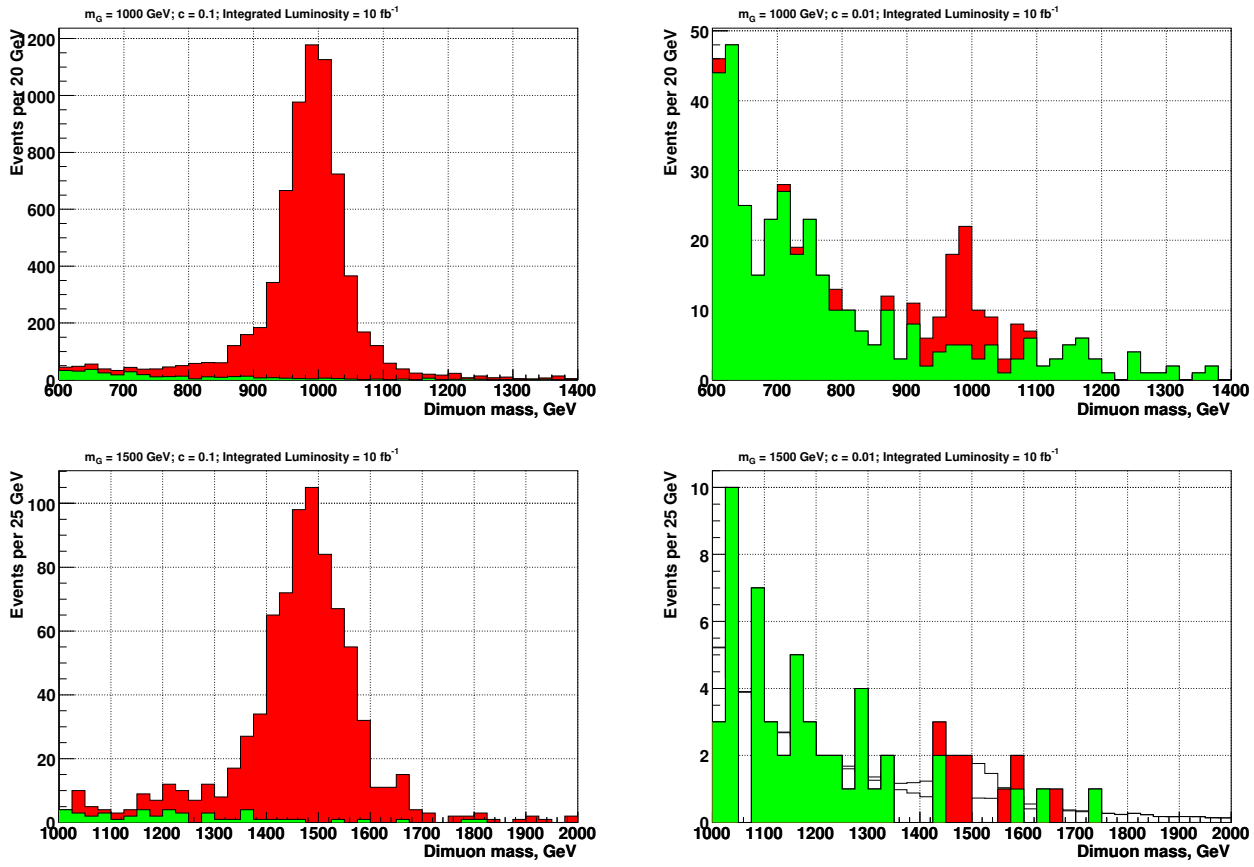

Figure 26: Reconstructed invariant mass distributions for RS1 graviton decaying into $\mu^+\mu^-$ pair. An example of Monte Carlo experiment is shown for integrated luminosity of 10 fb^{-1}: the signal (red dark area) is displayed over the background (green light area) for $m = 1000$ (top) and 1500 GeV (bottom). Left and right plots correspond to $c = 0.1$ and $c = 0.01$, respectively. Curves at the last plot show the limit of large statistics for the same integrated luminosity.

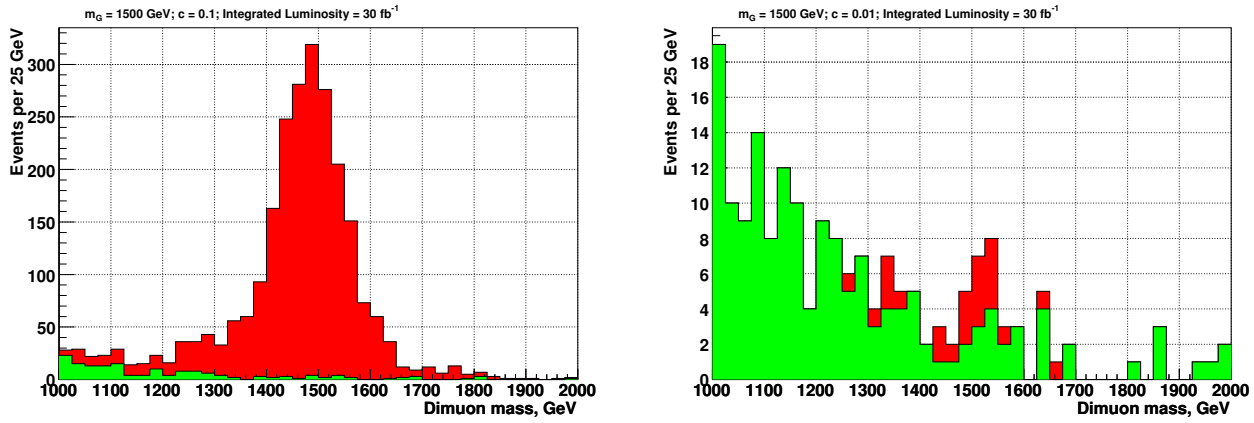

Figure 27: Reconstructed invariant mass distributions for RS1 graviton decaying into $\mu^+\mu^-$ pair. An example of Monte Carlo experiment is shown for integrated luminosity of 30 fb^{-1}: the signal (red dark area) is displayed over the background (green light area) for $m = 1500$ GeV. Left and right plots correspond to $c = 0.1$ and $c = 0.01$, respectively.

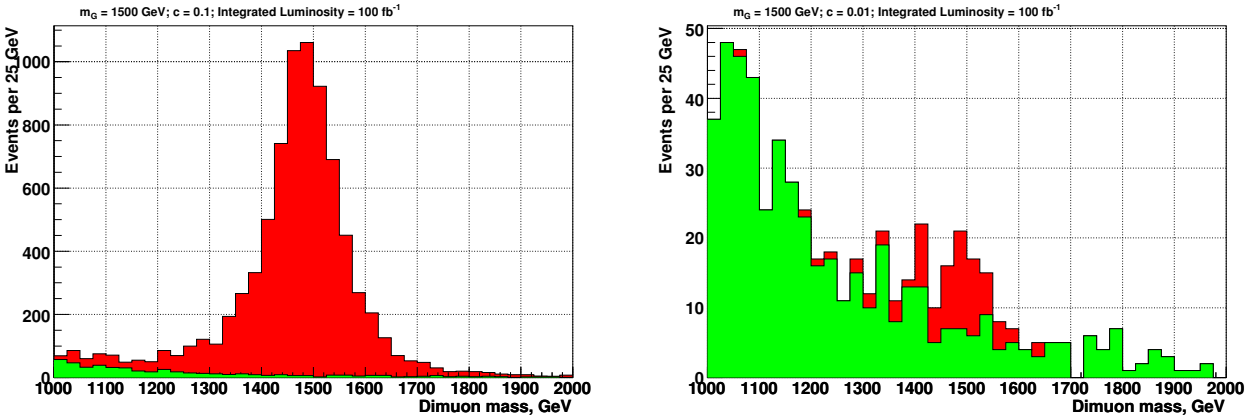

Figure 28: Reconstructed invariant mass distributions for RS1 graviton decaying into $\mu^+\mu^-$ pair. An example of Monte Carlo experiment is shown for integrated luminosity of 100 fb^{-1}: the signal (red dark area) is displayed over the background (green light area) for $m = 1500$ GeV. Left and right plots correspond to $c = 0.1$ and $c = 0.01$, respectively.